

**Preparation and Characterization of Whisker and
Particulate SiC-Al₂O₃ Ceramic Composites**

**By
Özlem Ebru ÜNVER**

**A Dissertation Submitted to the
Graduate School in the Partial Fulfillment of the
Requirements for the Degree of
MASTER OF SCIENCE**

**Department: Materials Science and Engineering
Major: Materials Science and Engineering**

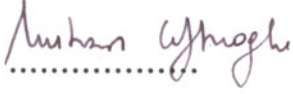
**Izmir Institute of Technology
Izmir, Turkey**

September , 1999

**İZMİR YÜKSEK TEKNOLOJİ ENSTİTÜSÜ
REKTÖRLÜĞÜ
Kütüphane ve Dokümantasyon Daire Bşk.**

We approve the thesis of Özlem Ebru ÜNVER

Date of Signature


.....

29.09.1999

Prof. Dr. Muhsin ÇİFTÇİOĞLU

Supervisor

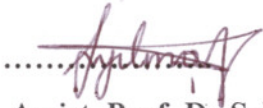
Department of Chemical Engineering,


.....

29.09.1999

Assist. Prof. Dr. Funda TIHMINLIOĞLU

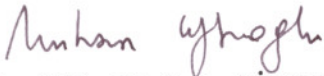
Department of Chemical Engineering,


.....

29.09.1999

Assist. Prof. Dr. Selahattin YILMAZ

Department of Chemical Engineering,


.....

Prof. Dr. Muhsin ÇİFTÇİOĞLU

Supervisor

Head of Interdisciplinary Materials Science
and Engineering Program

ACKNOWLEDGEMENTS

I would like to thank and express my gratitude to Prof.Dr. Muhsin Çiftçiođlu for his help and contributions during this study.

I also would like to express my thanks to Assist.Prof. Dr. Mustafa Guden for his valuable comments and suggestions, help and contributions during experimental work. Special thanks are to Uđur Ünal for help on computer problems and to research assistants for their friendship and to Hakan Ően for SEM pictures and to Özgenç Ebil for his help in cutting the samples. I am indebted to Nilgün Özgöl and Őerife Őahin for their help in the laboratory work.

Finally, I would like to thank to my husband Kemal Hakan Ünver and to my family, without which this thesis would be something different.

ABSTRACT

This work involves the preparation and the characterization of SiC particulate- Al_2O_3 and SiC whisker- Al_2O_3 ceramic composites. A new technique was used in order to increase the density of composite. Fine Al_2O_3 and SiC whiskers and particulates were used as a matrix and secondary phase, respectively. Whiskers and particulate were coated with Al-SO₄-OH precursor by precipitation using urea. In this method, it was important to keep the alumina hydrate in the noncrystalline state at $5.5 < \text{pH} < 8.6$. The alumina-hydrate compound was separated from SiC whiskers and particulates when the reaction was continued at high pH ($\text{pH} > 8.7$) causing the crystallization of alumina precursor. Alumina hydrate coated SiC whiskers and particulate were used as the starting material for the preparation of SiCw/p reinforced Al_2O_3 . Die pressing was used as the most appropriate and cheapest consolidation technique of composite materials. Upon sintering Al-SO₄-OH on the SiC transformed into Al_2O_3 by providing empty spaces for matrix densification in the proposed technique (shrink-fit idea). Green bodies with SiC whisker and particulate contents in the range of 10 to 40 vol.% were sintered at 1450°C for 2h under atmospheric conditions. The densities of sintered composites were measured by using Archimedes method. The density of composites containing 10%, 20%, 30% and 40 vol.% coated SiC particulate and whisker composites changed from 81% to 70% of theoretical density and from 79% to 75% of theoretical density, respectively. The density of coated composites were ~22% greater than that of the uncoated composites. The thermal behavior of Al-SO₄-OH on the SiC was characterized by using TGA, DTA. TGA curves showed that materials are hydrated and dehydroxylation was observed between $\sim 700^\circ$ and 800°C . TGA and DTA curves indicated that desulfurization then occurred at about $\sim 950^\circ\text{C}$. Chemical characterization of the coated SiC whiskers and particulates were obtained by using FTIR spectrometer.

The hardness of these composites were measured by using Vickers Microhardness Testing Device. Vickers microhardness of the 20vol.% and 30vol.% coated SiCp, and 20vol.% and 40 vol.% SiCw- Al_2O_3 composites were measured as 10.71, 12.94, 10.89 and 5.96 GPa, respectively and compared with the mechanical properties of the composites manufactured by the conventional methods.

ÖZ

Bu çalışma, SiC partikül- Al_2O_3 ve SiC whisker- Al_2O_3 kompozitlerinin hazırlanmasını ve karakterizasyonunu içermektedir. Bu kompozitler, yoğunluklarının artırılması amacıyla yeni bir teknikle hazırlanmıştır. Bu çalışmada, matriks olarak Al_2O_3 ve ikincil faz olarak da SiC whiskers yada partikülleri kullanılmaktadır. Whiskers ve partiküller üre yardımıyla çökeltme yöntemi kullanılarak Al-SO₄-OH bileşiğiyle kaplanmıştır. Bu yöntemde kaplamanın kristal yapıda olmaması önemlidir. Reaksiyon yüksek pH (pH>8.7) değerlerine kadar sürdürüldüğünde, Al-SO₄-OH bileşiği SiC whiskers ve partikülleri üzerinden sıyrılır ve kristal yapıya dönüşür. Al-SO₄-OH kaplı SiC whiskers ve partikülleri SiCw/p- Al_2O_3 kompozitlerinin hazırlanması için başlangıç malzemesi olarak kullanılmıştır. Hazırlanan toz karışım, en ekonomik ve en uygun yöntem olan soğuk presleme yöntemiyle şekillendirilmiştir. Sinterleme sırasında, Al-SO₄-OH bileşiğinin yoğunlaşarak Al_2O_3 fazına dönüşmesi ile matriks ve ikincil faz arasında boşluklar oluşturulur (Daralıp-Uyma). Bu yöntemle hazırlanan %10-%40 SiCw/p içeren bu kompozitler 1450⁰C'de 2 saat sinterlenmiş ve son yoğunlukları Archimedes yöntemi ile ölçülmüştür. Kaplanmış %10-%40 SiCw/p oranlarında hazırlanmış kompozitlerin yoğunlukları partikül kompozitleri için teorik yoğunluğunun %81-%70, whisker kompozitleri için %79-%75 olarak ölçülmüştür ve bu kompozitler aynı oranlarda hazırlanmış kaplanmamış kompozitler ile karşılaştırılmıştır. Kaplanmış kompozitlerin yoğunluklarının kaplanmamış kompozitlere oranla %22 daha yüksek olduğu görülmüştür. Al-SO₄-OH kaplı SiC whiskers ve partiküllerinin termal özellikleri TGA ve DTA analizleri yardımıyla belirlenmiştir. TGA analiz sonuçlarına göre kaplama malzemesi moleküler su içermektedir. DTA analizi yardımıyla da ~700⁰ ve ~800⁰C arasında dehydroxylation olduğu belirlenmiştir. Desülfürizasyon sıcaklığı ise hem DTA hemde TGA yardımıyla ~950⁰C olarak elde edilmiştir. Kaplanmış whisker ve partiküllerin kimyasal karakterizasyonu FTIR cihazı yardımıyla yapılmıştır.

Çökeltme yöntemi ile hazırlanan kompozitlerin sertlik değerleri Vickers mikrosertlik cihazı ile ölçülmüş ve %20,%30 SiCp- Al_2O_3 kompozitleri için sırasıyla 10.71, 12.94 ve %20,%40 SiCw- Al_2O_3 kompozitleri için ise 10.89 ve 5.96 Gpa bulunmuştur. Bu değerler literatürdeki değerler ile kıyaslanmıştır.

TABLE OF CONTENTS

| | |
|---|------|
| LIST OF TABLES | vii |
| LIST OF FIGURES | viii |
| | |
| I. INTRODUCTION | 1 |
| | |
| II. CERAMIC PROCESSING | 4 |
| 2.1 Raw Materials Preparation | 4 |
| 2.2 Forming Processes | 4 |
| 2.3 High Temperature Treatment | 8 |
| 2.3.1 Stages of Sintering | 8 |
| | |
| III. CERAMIC MATRIX COMPOSITES | 14 |
| 3.1 Whisker Reinforced Ceramic Matrix Composites | 14 |
| 3.2 Particle Reinforced Ceramic Matrix Composites | 16 |
| 3.3 Reinforcement Mechanism | 17 |
| 3.3.1 Transformation Toughening | 17 |
| 3.3.2 Crack Bridging | 18 |
| 3.3.3 Microcracking | 19 |
| 3.3.4 Crack Deflection | 20 |
| 3.3.5 Fiber Reinforcement | 20 |
| 3.4 Interfaces in Composites | 22 |
| 3.4.1 Interface Design Parameters | 22 |
| 3.4.2. Fiber-Matrix Debonding | 25 |
| 3.4.3 Fiber Pull-Out | 26 |
| 3.4.4 Interface Formation | 26 |

| | |
|---|----|
| IV. COATING OF POWDERS | 29 |
| 4.1 Chemical Solution Techniques | 29 |
| 4.1.1 Chemical Precipitation Technique | 29 |
| 4.2 Coating of SiC Whiskers and Particulates with Al ₂ O ₃ | 32 |
| 4.3 Shrink-Fit Idea | 34 |
| IV. EXPERIMENTAL WORK | 37 |
| 5.1 Preparation of Coated SiC _w and SiC _p | 37 |
| 5.2 Composite Preparation and Consolidation | 39 |
| 5.3 Sample Preparation For Microhardness Test | 41 |
| VI. RESULTS AND DISSCUSION | 43 |
| 6.1 Preparation of Alumina Hydrate-coated SiC whiskers and SiC particulates | 43 |
| 6.2 Effect of SiC Whiskers and Particulates on Densification | 51 |
| 6.3 Density Measurements | 54 |
| 6.4 Thermal Analysis | 62 |
| 6.5 Chemical Characterization | 66 |
| 6.6 Vickers Microhardness Test Results | 73 |
| CONCLUSIONS AND RECOMMENDATIONS | 75 |
| APPENDIX | 78 |
| REFERENCES | 80 |

LIST OF TABLES

| | |
|--|----|
| Table 1. Effect of uncoated SiC particulates on sintering | 56 |
| Table 2. Effect of coated SiC particulates on sintering | 57 |
| Table 3. Effect of uncoated SiC whiskers on sintering | 58 |
| Table 4. Effect of coated SiC whiskers on sintering | 59 |
| Table 5. Effect of 1100 °C calcined coated SiC particulates on sintering | 60 |
| Table 6. Effect of 1100 °C calcined coated SiC whiskers on sintering | 61 |
| Table 7. Vickers Microhardness test results of the SiC-Al ₂ O ₃ composites | 73 |

LIST OF FIGURES

| | |
|--|----|
| Figure 1. A schematic representation of die-pressing | 6 |
| Figure 2. A schematic representation of slip casting | 7 |
| Figure 3. Changes that occur during the initial stage of sintering | 9 |
| Figure 4..Changes that occur during the second stage of sintering | 10 |
| Figure 5. Changes that occur during the final stage sintering | 11 |
| Figure 6. Optical micrograph of 20% SiC _w -Si ₃ N ₄ composite prepared by slip casting | 15 |
| Figure 7. Strength and toughness of SiC-Al ₂ O ₃ composites for two different particle sizes | 17 |
| Figure 8. A schematic representation of transformation toughening | 18 |
| Figure 9. A schematic representation of crack bridging | 19 |
| Figure 10. A schematic representation of microcracking | 19 |
| Figure 11. A schematic representation of crack deflection | 20 |
| Figure 12. Schematic of a fracture crack in a ID composite | 21 |
| Figure13. Debond characteristics for Brittle matrix composites | 23 |
| Figure 14. Schematic of matrix microcracking | 24 |
| Figure 15. Schematic of fiber debonding | 25 |
| Figure 16. Schematic representation of fiber pull-out | 26 |
| Figure 17. Transmission electron micrograph of the interfacial region of a lithium-alumino-silicate matrix and Nicalon TM SiC fiber | 27 |
| Figure 18. Transmission electron micrograph of the interfacial zone fiber-matrix in a SiC-SiC composite | 28 |
| Figure 19. Processing flow diagram for the preparation of a pure precipitate | 30 |
| Figure 20. Single component coating powder by heterogeneous Precipitation | 31 |
| Figure 21. Multicomponent coating | 31 |

| | |
|--|----|
| Figure 22. Schematic representation of shrink-fit idea | 36 |
| Figure 23. The preparation procedures for alumina hydrate coated SiC whiskers and particulates | 39 |
| Figure 24. The preparation of alumina hydrate coated SiC whiskers and particulates- Al_2O_3 composites | 40 |
| Figure 25. Schematic representation of sample preparation of microhardness test | 41 |
| Figure 26. Aluminium sulfate hydrate spherical particles | 44 |
| Figure 27. Reflected optical micrographs of uncoated SiC particulates (particle size $\sim 20\mu\text{m}$) | 44 |
| Figure 28. Reflected optical micrographs of the morphology of the Precipitates | 45 |
| Figure 29. Scanning electron micrographs of uncoated SiC whiskers | 46 |
| Figure 30. Reflected optical micrographs of alumina hydrate coated SiC whiskers at different pH values | 46 |
| Figure 31. pH curve for SiCp | 47 |
| Figure 32. Scanning electron micrographs of alumina hydrate coated SiC particulates | 48 |
| Figure 33. Reflected optical micrographs of alumina hydrate coated SiC Whiskers | 48 |
| Figure 34. X-Ray Diffraction patterns for uncoated SiC particulates | 49 |
| Figure 35. Scanning electron micrographs of coated SiC particulates at $\text{pH} > 8.6$ | 50 |
| Figure 36. Scanning electron micrographs of coated SiC whiskers at $\text{pH} > 8.6$ | 50 |
| Figure 37. Fracture surface of Al_2O_3 produced by die-pressed and sintered at 1450°C for 2h | 51 |
| Figure 38. Scanning electron micrograph of fracture surface of 20 vol.% SiC whisker- Al_2O_3 | 52 |

| | |
|--|----|
| Figure 39. Scanning electron micrograph of fracture surface of 20 vol.% SiC particulate- Al ₂ O ₃ | 53 |
| Figure 40. Effect of uncoated SiC particulates on densification of Al ₂ O ₃ matrix composites | 56 |
| Figure 41. Effect of coated SiC particulates on densification of Al ₂ O ₃ matrix composites | 57 |
| Figure 42. Effect of uncoated SiC whiskers on densification of Al ₂ O ₃ matrix composites | 58 |
| Figure 43. Effect of coated SiC whiskers on densification of Al ₂ O ₃ matrix composites | 59 |
| Figure 44. Effect of 1100 ⁰ C calcined coated SiC particulates on densification of Al ₂ O ₃ matrix composites | 60 |
| Figure 45. Effect of 1100 ⁰ C calcined coated SiC whiskers on densification of Al ₂ O ₃ matrix composites | 61 |
| Figure 46. TGA curve for coated SiC particulates | 64 |
| Figure 47. TGA curve for coated SiC whiskers | 65 |
| Figure 48. FTIR spectrum of coated SiC particulates | 69 |
| Figure 49. FTIR spectrum of coated SiC whiskers | 70 |
| Figure 50. DTA curve for alumina hydrate coated SiC particulates | 71 |
| Figure 51. DTA curve for alumina hydrate coated SiC whiskers | 72 |
| Figure 52. A schematic illustration for the density measurements. | 79 |

CHAPTER I

INTRODUCTION

Ceramic science may be defined as the art and science of making and using solid articles of inorganic, non-metallic materials. This broad definition of ceramics comprises not only traditional ceramics (dishes, tiles and bricks) but also advanced engineering ceramics of oxides (Al_2O_3 , ZrO_2 , ThO_2 , BeO , MgO), magnetics ($\text{PbFe}_{12}\text{O}_{19}$, ZnFe_2O_4 , $\text{Y}_6\text{Fe}_{10}\text{O}_{24}$), ferroelectrics (BaTiO_3), nuclear fuels (UO_2 , UN), nitrides, carbides and borides (Si_3N_4 , B_4C , and TiB_2).

Traditional ceramics are manufactured by mixing and processing of three basic raw materials: clay, silica (flint) and feldspars. The processing techniques of traditional ceramics are relatively simple and some date backed to early ages, before 5000 BC. Shaping forming and firing of ceramic raw materials using potter's wheel and closed kilns were explored in those ages and are also common in today's traditional ceramic processing.

Progresses in understanding, refining and synthesising of ceramic raw materials in the second half of the 20th century lead to a new area of ceramics called advanced ceramics. These ceramics can be engineered to highly controlled compositions and structures to fill specific needs of continuing technological progress of 20th century in many areas, which would otherwise could not be filled by other available materials. Some of the important properties of advanced ceramics over the metals and polymers include excellent chemical and corrosion resistance to severe environments, optical transparency, higher modulus, hardness and resistance to wear. Application areas of advanced ceramics include electronics such as dielectric materials, substrates, semiconductors, and transducers, medical materials such as prosthetics and orthodontics and structural materials such as turbine components and heat exchangers (24,26).

Structural applications of monolithic ceramics are, however, imparted by the inherent low toughness or lack of ductility. Under external tensile forces, cracks start from porosities, microcracks and machining flaw on the surface, and propagate quickly. Unlike monolithic ceramics, fiber reinforced ceramic

composites (CMCs) fails in a non-catastrophic manner. This is primarily promoted by the large work of fracture to pull broken fibers against frictional sliding resistance between fiber and matrix and by the crack deflection at interfaces. Based on experimental studies on CMCs, following criteria can be used to establish tough composites: low toughness interface, low interface sliding and low thermal mismatch stresses (7). Therefore, interface design in CMCs is a major issue of processing of these materials. Current efforts are concentrated on in-situ reactions at interfaces and coating of fibers.

In-situ reactions are widely used in fiber reinforced glass matrix ceramic composites. For example in Nicalon fiber (Si-C-O) reinforced LAS (LiO-Al₂O₃-SiO₂) composite, a weak carbon rich interfacial zone is formed by the oxidation of the SiC fiber surface during hot pressing step. In the second approach, interface is formed on the surface of the fiber prior to composite fabrication, for example BN and C coating on SiC fibers in glass matrix composites (8). In the design of interfaces, in both in-situ formed and coated interfaces, thermal residual stresses must be considered carefully, because they may induce microcracking in the composites which may reduce the fracture toughness and strength of the final composite structure.

Their high strength, wear resistance, capability of preserving their strength at high temperatures and their resistance to creep are some of the important mechanical negativens of ceramic materials that cause brittle structure, in another words causing their toughness being low. The main goal of ceramic composite materials is partially improved. In a study on Al₂O₃ matrix composite material, the fracture toughness of a ceramic composite with 30 vol.% SiC whisker is increased almost two times (relative to the fracture toughness of pure Al₂O₃) with the density (29,30). The other factors that affect the increase in toughness in ceramic composites are: volume content of whiskers/particulates, homogeneous distribution of whiskers/particulates and density of composite (6). For the distribution of whiskers, various methods are employed. The most significant of these are: to obtain a good distribution of whiskers by using deflocculants (2) or by electrostatic stabilization of whiskers (12).

The most important reason of density decrease in the composites is the thermal stresses, microcracks and cavities that occur during heating and cooling. In many ceramic composites, matrix has a higher coefficient of thermal expansion than the reinforcement; therefore, interface remains under tensional stresses. To prevent this effect, an empty space at fiber matrix interface for the matrix growth during high temperature processing of composite, known as "shrink-fit", is proposed. The thermal stresses are due to the differences in thermal expansion coefficients. Subsequently this difference within the matrix and second phase cause the pull stress in the matrix during the sintering. Irregular distribution of second phase cause different stresses, which creates huge cavities. This is the reason for the extraordinary extension of the particles in the composite where the density of whisker is less. Cavities that are stuck inside expand particles that cannot shrink. In order to prevent these effects, whiskers/particulates are coated with polymers which are burned before densification and subsequently the gap is created between the matrix and whiskers/particulates (32).

In this study, in order to create a gap between whiskers/particulates and the matrix, whiskers/particulates are coated with an aluminium-sulfate-hydrate compound. Coating of reinforcement prior to consolidation of the composite constituents was to form a space or a gap between reinforcement/matrix interface for matrix growth. This was achieved by the shrinkage of the coating on the reinforcement surface during the heating of the consolidated green body to high temperatures. With this method, it was aimed in this study that the content of microcracks formed in the matrix due to difference between the coefficient of thermal expansion of matrix and reinforcement would be reduced.

CHAPTER II

CERAMIC PROCESSING

There are three main stages in ceramic processing: These are raw materials preparation, compaction and densification.

2.1. Raw Materials Preparation

Powder preparation is one of the most basic steps of ceramic processing. Chemical and phase purity are two basic requirements for subsequent processing of powders. It is also often desired to have particles consisting of individual rather than multiple crystallites and for a number of applications; particles of individual crystallites having crystallographic shapes are desired. Particle size control and distribution are necessary in order to optimise properties of the intended final ceramic product.

Many different mechanical size reduction and chemical preparation techniques have been developed to achieve the above requirements. Some of the mechanical size reduction techniques are screening, ball milling, roll crushing and air classification. Precipitation, sol-gel technique, decomposition and plasma processing are the most important chemical preparation techniques (24).

2.2. Forming Processes

Following the preparation stage, ceramic powder is consolidated into desired shapes using one of the following techniques: pressing, slip casting and

injection molding. The selection of the suitable forming technique depends on several factors such as the size, shape, dimensional tolerances of the product, the levels of reproducibility required, and investment and productivity considerations.

Pressing is accomplished by placing a powder which is premixed with suitable binders and lubricants into a die and applying pressure for compaction. In pressing, two techniques are essentially distinguished: die pressing in which a certain amount of powder is put into a die and shaped by the punches under a load and iso-static pressing in which a powder batch is consolidated by an iso-static pressure applied by a fluid on a pre-shaped compact, provided with an impermeable cover.

In powder pressing the powder is either completely dry or contains up to 5 %vol. water. Water addition improves the adhesion of the powder. Binders are added, if necessary. Binders such as "dextrine" and "acrylate" are called hard binders and wax and Arab gum are soft binders. Polyvinyl alcohol or methylcellulose are intermediate binders. In order to reduce frictional effects of the die, lubricants such as paraffin oil or stearine solution are sometimes added with an amount of a few tenths of a percent.

Die pressing is used extensively in the compaction of refractories, tiles, special electrical and magnetic ceramics, spark plug insulators and other technical ceramics for which large numbers of simple shapes are required. The method is relatively cheap and used to form shapes with close tolerances. Pressures ranging from 35 to 105 MPa are common and the higher pressures may be suitable for the harder materials such as pure oxides and carbides (Figure 1).

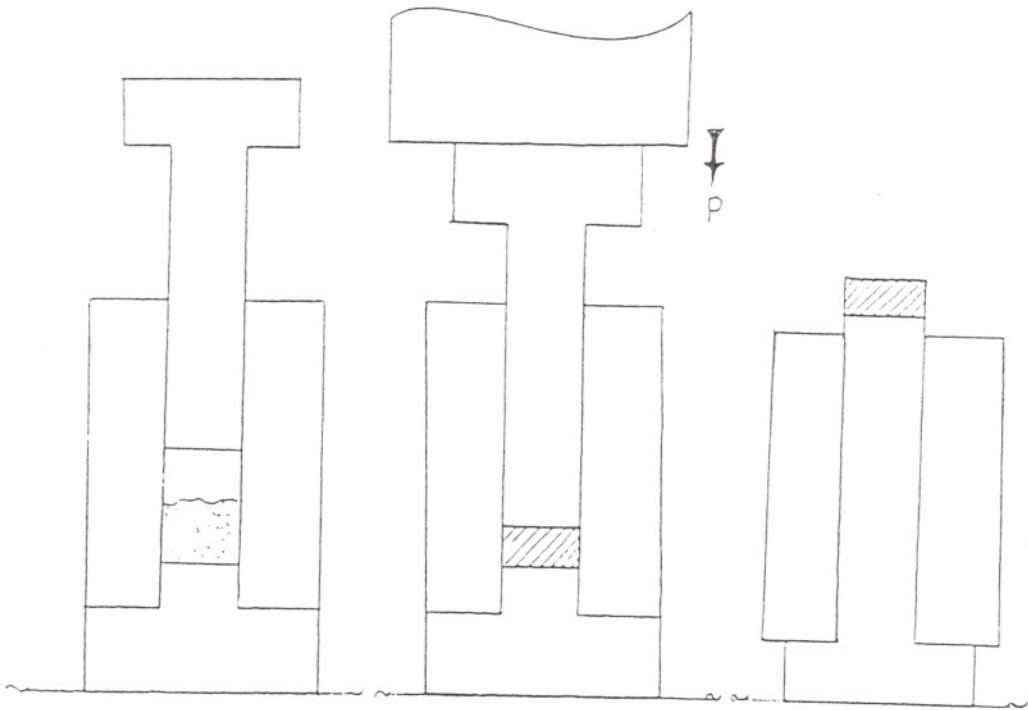


Figure 1. A schematic representation of die-pressing.

Although it is a simple and useful tool of ceramic powder forming technique, die pressing suffers from some limitations. Filling the mold with powder and transmitting pressure to all parts of the mold cavity are critical to obtain uniform dense compacts without weak edges. Variation of pressure during compaction and density gradients in the green body generally result in variations in fired density and uneven shrinkage. Therefore, the ratio of the length in the direction of the pressing to the diameter is limited.

A slip can be defined as a stable dispersion with a high volume fraction of solid particles (45-60%) in a liquid, usually water. The fluidity of the slip is provided by adding deflocculants. The slip is cast in a porous plaster mold to form a compact section along the walls. When the wall thickness of the compact is large enough or the growth of the wall thickness is largely stopped by saturation of the mold, remaining slip is drained. The casting is then removed after partial drying (Figure2).

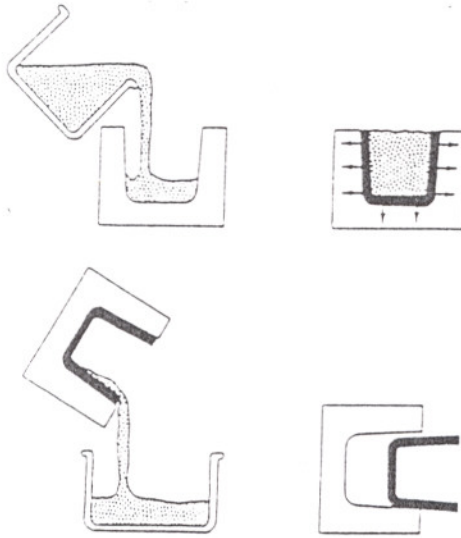


Figure 2. A schematic representation of slip casting.

A bubble free high density compact is an indication of a stable slip. For a good casting process a well-prepared slip, however, is not enough; the mold must be such that it will allow the water to be withdrawn evenly through its porous walls. The mold must also be designed to allow shrinkages by the end of casting. For the easy removal of the last piece finally, the part must have sufficient strength so that it can be handled and can be removed from the mold without cracking .

Slip casting is a relatively simple and flexible technique of ceramic forming. It is frequently used in laboratory, while modifications such as tape casting and pressure casting are mostly used in factory practice. Complicated shapes can be produced by using multi part molds at a relatively low cost although the production rate may be relatively low (5,24,26).

2.3 High Temperature Treatment

High temperature treatment involves drying, sintering, and vitrification and form the final and major step in ceramic processing.

Drying of ceramics is the removal of water from the green compacts before firing. Drying is usually carried out at/or above 100 °C. The bulk of organic binders can, however, be removed in the temperature range of 200 to 300°C and hydrocarbon residues may further require much higher temperatures.

Some ceramic products including porcelain, structural clay products and electronic components contain glass phase. The formation of a liquid phase serves as a reaction medium by which diffusion can take place at a low temperature than in the rest of the solid. During the firing of these types of ceramics, the glass phase liquid forms and fills the pore spaces in the material. This is called vitrification or liquid phase sintering. Upon cooling the liquid glass phase solidifies to form a vitreous or glassy matrix that bonds the unmelted particles together (28).

Solid state sintering is a technical term referring to densification of ceramic compacts at relatively high temperatures. It removes pores between the particles by combining particles, allowing particles to grow together and forming strong bonding between adjacent particles. Decomposition or transformations of phases may occur during sintering. In addition to phase decomposition, changes in grain size, pore shape and size content occurs during sintering.

2.3.1 Stages of Sintering

The initial stage of sintering involves rearrangement of particles and formation of necks at the contact points of particles. Bonding occurs at the contact points and slight movement or rotation of adjacent particles increases the

number of contact points. The changes that occur during the first stage of sintering are illustrated in Figure 3.

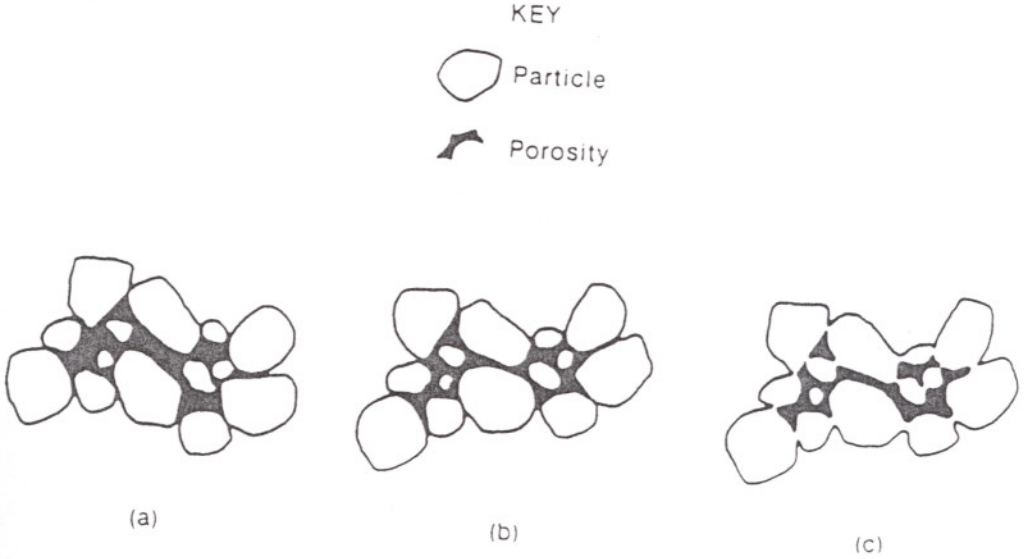


Figure 3 Changes that occur during the initial stage of sintering.

(a) Starting particles, (b) rearrangement, and (c) neck formation.

In the second stage of sintering, the size of the necks between particles grows. Porosity decreases as the centers of the original particles move closer together. This results in shrinkage equivalent to the amount of porosity decrease. The grain boundaries begin to move so that one particle (now called grain) begins to grow while the adjacent grain is consumed. Most of the shrinkage during sintering occurs during second-stage of sintering (Figure 4).

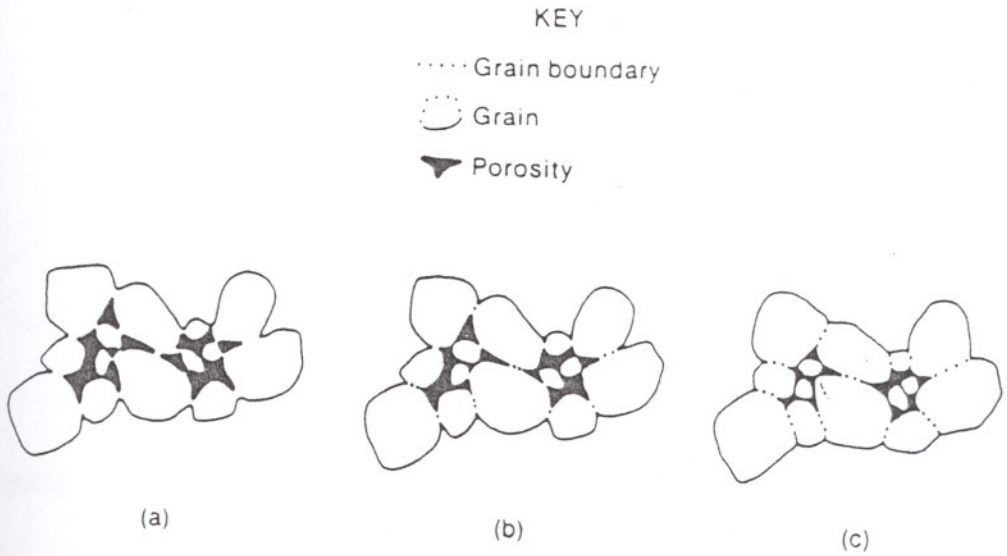


Figure 4. Changes that occur during the second stage of sintering.

- (a) Neck growth and volume shrinkage,
- (b) lengthening of grain boundaries, and
- (c) continued neck growth and grain boundary lengthening, volume shrinkage, and grain growth.

The third stage of sintering involves the removal of final porosity. The porosity is removed via vacancy diffusion aided by movement of grain boundaries and controlled grain growth. If grain growth is too fast, the grain boundaries move faster than the pores and leave them isolated inside a grain (intragranular). If the necessary transport processes are sufficiently rapid along grain boundaries, so pores must remain attached to a boundary (intergranular) in order to be eliminated (Figure 5).

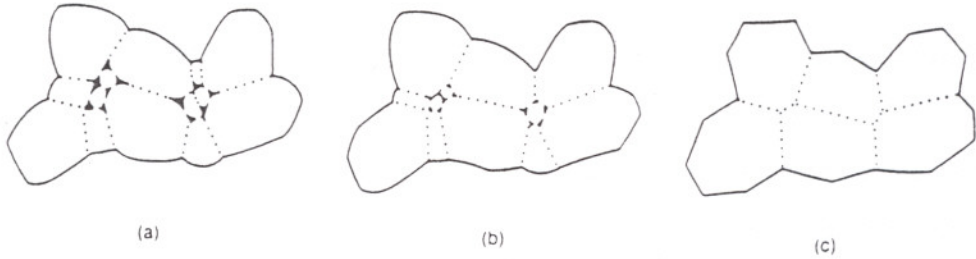


Figure 5. Changes that occur during the final stage of sintering.

- (a) Grain growth with discontinuous pore phase,
- (b) grain growth with porosity reduction,
- (c) grain growth with porosity elimination.

Before firing, a powder compact is composed of individual grains separated by 25 to 60 volume percent porosity, depending on the particular material and the processing method used. For maximizing properties such as strength, translucency, and thermal conductivity, it is desirable to eliminate as much of this porosity as possible.

Traditional oxide ceramics are readily sinterable because of the formation of liquid phases. Some higher technology oxides are processed with additives to provide liquid phase sintering and to enhance solid-state sintering or to retard grain growth. Many nonoxides such as SiC and Si₃N₄ can only be sintered with additives.

If a suitable additive system can be identified for a ceramic system that can promote densification without external pressure (pressureless sintering), then this is the preferred method since complex-shape components can be densified rather easily and cheaply in this manner. Besides pressureless sintering, there are four modified densification processes: reaction sintering, overpressure sintering, hot pressing and hot isostatic pressing. In these

processes pressure is applied simultaneously with heating. The application of pressure increases the energy at the particle-particle contacts and thus enhances the normal mechanisms of sintering. Densification of consolidated powder bodies is achieved predominantly by pressureless sintering. However, the use of hot pressing is increasing, especially for oxides and parts of simple shapes where higher quality (mainly microstructural homogeneity) is needed. Moreover, larger size or multiple parts per pressing can be an additional advantage. The use of hot isostatic pressing is increasing, especially following sintering to closed porosity, and where quality and complexity of shape justify the cost. There are also important opportunities to make quality ceramic products using lower cost ingredients, by sintering or hot pressing, for example, by reaction sintering (24,26).

Alumina (Al_2O_3) has mechanical, thermal and electrical properties superior to most other oxide ceramics. Moreover, the raw materials are plentiful, cheap, and accommodating better to fabrication by a variety of techniques into a wide variety of shapes. Although alumina presents a number of metastable structures, they all transform irreversibly to hexagonal alpha phase of technological interest.

The properties of the alumina ceramics meet many engineering requirements of electrical applications ranging from packages for electronics, plasma envelopes for some gas lasers to radomes and microwave components to high strength insulators in the electric power distribution industry and spark plugs in gasoline engines. Wear applications include noncontaminating grinding media, mud pump liners, mechanical seals, textile and wire guides. High temperature applications range from plasma torch insulators to compression springs.

Silicon carbide is one of the most corrosion resistant ceramics, being almost totally resistant to acids and bases. Its structure consists of a tetrahedron which may be considered to be presented as a silicon atom bonded to four carbon atoms, or conversely carbon atoms bonded to four silicon atoms. The difference in the orientation by which the tetrahedra are stacked make a number of crystal polytypes possible. There is a very slight density difference depending upon tetrahedral stacking.

Applications, such as abrasives, refractories as well as electrical industry. If the mechanical properties can be improved, new application areas like including fixed and rotating turbine components, liners for hot gas flow, rocket nozzles and heat exchangers will develop (5,13,26).

İZMİR YÜKSEK TEKNOLOJİ ENSTİTÜSÜ
REKTÖRLÜĞÜ
Kütüphane ve Dokümantasyon Daire Bşk.

CHAPTER III

CERAMIC MATRIX COMPOSITES

The intrinsic high stiffness, high hardness, chemical inertness and refractoriness of ceramics derive from their ionic and covalent bonding structures. These bonds permit little or no movement of dislocations, even at high temperatures, and leads ultimately to brittleness or lack of toughness. In many applications involving at relatively high temperature, ceramics both tough and resistant to high temperatures are, however, needed. Ceramic matrix composites (CMCs) can potentially meet these requirements when reinforced by particles or fibers and/or whiskers and tailored for energy dissipating mechanical events such as fiber debonding and fiber pull-out.

3.1 Whisker Reinforced Ceramic Matrix Composites

Whiskers are the single crystalline fibers having diameters in the range of 0.1-1 μm and aspect ratios (length/diameter) of 10-100. The absence of grain boundaries and high purity bring up several attractive characteristics. They exhibit a good chemical stability at ambient and relatively high temperatures. Due to small size, they contain only small size defects; therefore, they can show high tensile strength values. The average strength values of whiskers have been measured to be about 8 GPa ($\phi=6\mu\text{m}$) (21).

Several types of whiskers have been used for the reinforcement of ceramics. These include silicon carbide, silicon nitride and alumina; however, only silicon carbide has been widely developed and tested.

Whisker addition usually reduces the densification; therefore hot pressing (HP) is mostly used for the preparation of whisker reinforced ceramic composites. HP results in a planar random whisker orientation: whiskers are randomly oriented in the planes normal to the pressing direction. This is also

true for the composites formed by slip casting technique in which whiskers are randomly oriented in planes parallel to the slip mold interface (Figure 6).

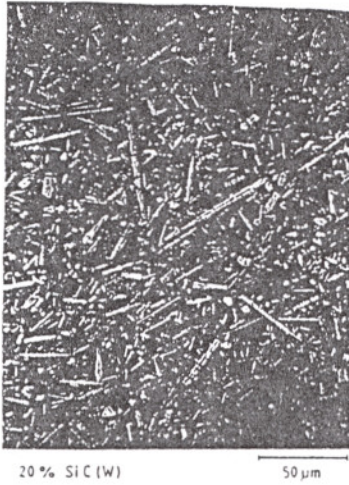


Figure 6. Optical micrograph of 20 % SiC_w-Si₃N₄ composite made by slip casting. Note that whiskers are randomly oriented in planes (3).

The structural anisotropy in these composites have been observed on the microstructure. The anisotropy is also reflected by the relatively large differences between the toughness and strength values of crack planes perpendicular and parallel to the whisker plane (3). On a macroscale, isotropic bodies can be, however, obtained by powder preparation and pressureless or hot isostatic pressing (HIP).

The importance of aspect ratio has not been widely explored. Both the strength and the toughness were found to increase; from 380 to 560 MPa for strength and from 4,7-5,3 MPa.m^{1/2} for toughness. Fracture surface observations showed that longer whiskers experienced more extended pull-out. They also found that toughness values over 9 MPa.m^{1/2} were possible when the whisker content increased (1).

3.2 Particle Reinforced Ceramic Matrix Ceramics

The development of such composite materials was primarily focused on tribological applications. The target is to improve both toughness and hardness. Typical matrix and reinforcement couples are:

- Reinforcement of alumina by SiC, TiC, BN and TiN;
- Reinforcement of silicon carbide by TiB₂, TiC and AlN; and
- Reinforcement of silicon nitride by SiC and TiC.

Since the residual stress due to coefficient of thermal expansion (CTE) mismatch is an important parameter controlling the toughening, it is convenient to classify those composite materials into three different groups:

$\alpha_p > \alpha_m$: TiC-SiC, SiC-Si₃N₄, TiC- Si₃N₄,

$\alpha_p \cong \alpha_m$: TiB₂-SiC, TiC-Al₂O₃, AlN-SiC,

$\alpha_p < \alpha_m$: SiC-Al₂O₃, BN- Al₂O₃.

Materials from the last category ($\alpha_p < \alpha_m$) are more susceptible to experience microcrack toughening where the probability of microcracking is low and toughening will be mostly due to crack-particle interaction.

In particle reinforced CMCs, toughness is a function of particle content and size content. In a study on SiC_{particle}- Al₂O₃ composite with two reinforcement sizes 2 and 8 μ m, the highest toughening has been obtained with the smaller particle and materials exhibit a maximum toughness as a function of the particle content. (Figure 7) (5).

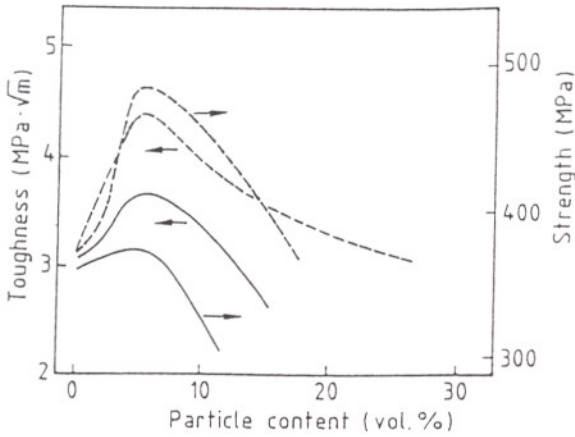


Figure 7. Strength and toughness of SiC-Al₂O₃ composites for two different particle sizes: solid line: 8μm, dashed line: 2μm (5).

3.3 Reinforcement Mechanism

Reliability of a ceramic component is majorly affected by the fracture toughness and most ceramics show inherently little plastic deformation prior to fracture. A number of methods have been developed in the last 25 years to increase the fracture toughness of ceramics including: transformation toughening, crack bridging, crack deflection, micro-cracking and fiber reinforcement.

3.3.1 Transformation Toughening

Transformation toughening is based upon a martensitic phase change in a second phase inclusion that leads to an increase in the inclusion volume during transformation. The ceramics containing zirconia particles which presents tetragonal to monoclinic phase transformation is the most spectacular.

In these composites, the zirconia particles are dispersed in the matrix and the composite is densified at 1000 to 1700⁰C where the tetragonal zirconia phase is thermodynamically stable. Upon cooling below 800⁰C, the monoclinic phase become stable but the volume is 7% larger per unit mass and it is restrained from transforming by the matrix. The expansion during the transformation tends to push the crack closed lowering the driving force for further crack propagation resulting in a higher material toughness. (Figure 8)

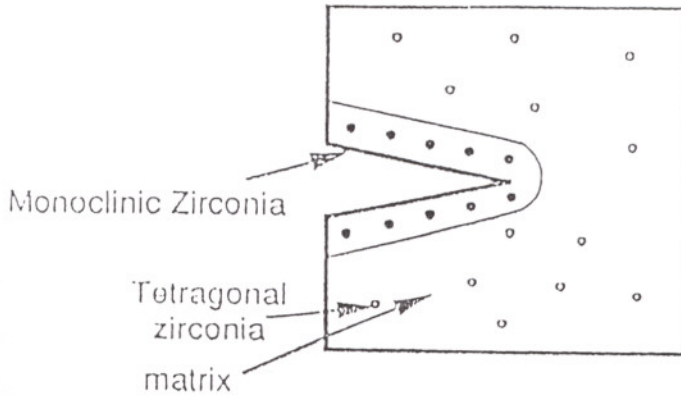


Figure 8. A schematic representation of transformation toughening.

3.3.2 Crack Bridging

When a crack goes around a reinforcement without breaking it, crack bridging occurs. In order to obtain a high reinforcement, one must maximize the reinforcement strength and radius and minimize the interface bonding strength (Figure9).

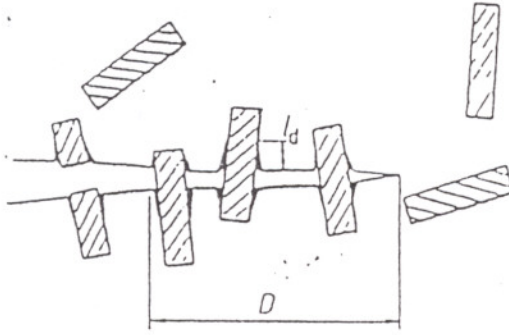


Figure 9. A schematic representation of crack bridging.

3.3.3 Microcracking

When loading the material owing to the stress field present around the particles, it can absorb elastic energy and thus contribute a fracture energy increase so microcracking can be induced. Cracking occurs only around the particles greater than a critical size, this shows that the elastic energy (due to thermal contraction mismatch) is stored in the matrix and the particle must be greater than the surface energy needed to create the crack (Figure 10).

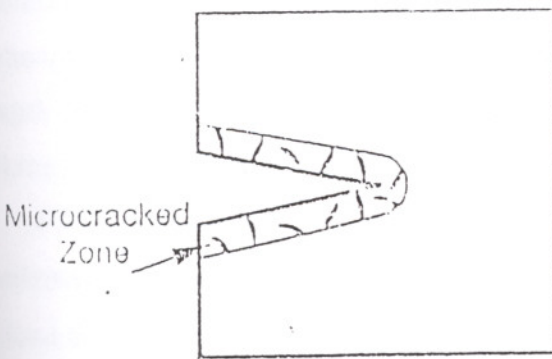


Figure 10. A schematic representation of microcracking.

3.3.4 Crack Deflection

Crack deflection can be achieved either by stress field present around particles or by hard particles of higher resistance. (Figure 11)

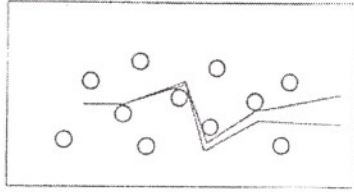


Figure 11. A schematic representation of crack deflection.

3.3.5 Fiber Reinforcement

The fundamental reinforcement mechanisms of fiber composites are dominated by the interface between the fiber and the matrix. These basic mechanisms are governed mainly by the relative fiber-matrix interface debond toughness, the friction coefficient, the thermal residual stresses, the fiber strength distribution, the matrix properties (such as toughness and matrix cracking) and the fiber volume fraction.

Fibers introduced in a matrix lead to two effects: thermal stresses due to the mismatch of the coefficient of thermal expansion of fiber α_f and matrix α_m and load transfer involving the fiber-matrix interface. If $\alpha_f < \alpha_m$, the interface is in compression and there is a fretting of the fiber. If $\alpha_f > \alpha_m$, the matrix is compressed but the interface is in tension, leading to very poor load transfer. Control of the interface properties (thermal stresses, friction conditions) can be achieved by using either coatings or in-situ reactions between the fibers and the

matrix. Further discussion on interfacial behavior is provided in section 3.4 of this chapter.

For ceramic matrix, generally fracture strain of the matrix ϵ_m is lower than that of the fiber ϵ_f . Thus, the microcracking starts in the matrix if the fiber fraction is higher than the critical V_f . and there is a load transfer from the matrix to fibers through a shear stress τ_i at the fiber matrix interface. These stress profiles, after matrix cracking depend on the interface behavior. A more accurate analysis must take into account the residual thermal stresses, debonding and the statistical nature of matrix and fiber fracture. In the case of matrix microcracking and bonded interface, the interfacial stresses can lead to a debonding phenomenon.

So, when a main crack propagates in a 1D composite, fibers bridge between the crack surfaces and different zones can be observed (Figure 12).

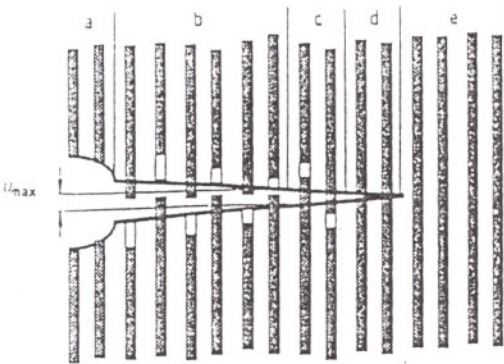


Figure 12. Schematic of a fracture crack in an ID composite.

The zone a is the notch. In zone b, no interaction between the crack surfaces occurs (all the fibers are pulled out) . In zone c, the crack is bridged by broken fibers whereas unbroken fibers intervene in zone d. The zone e is undamaged.

3.4 Interfaces in Composites

Interface in fiber reinforced composites may be defined as a surface formed by the common boundary of reinforcing fiber and matrix. It has physical and mechanical properties which are unique and not either of those of the fiber nor the matrix. It is usually considered to be zero thickness (or volume) and perfectly bonded.

The structure and properties of fiber-matrix interface play a major role on the mechanical performance and structural integrity of composite materials. A bond is formed between a chemical grouping on the fiber surface and a chemical group in the matrix and bond strength depends on the number and type of bonds, the formation of which are usually thermally activated chemical reaction. In most ceramic matrix composites, chemical reaction hardly occurs between fiber and matrix. However, an extremely thin amorphous film can be formed originating from the oxide present on the fiber surfaces or due to the limited fiber-matrix interaction, e.g., between alumina whisker and zirconia matrix (30). Mechanical bonds involve mechanical interlocking at the surface. There are many internal and residual stresses in composite materials which develop during fabrication processes due to matrix shrinkage and differential thermal expansion between fiber and matrix. Among these stresses, the residual clamping stress on the fiber provides a major bonding at the interface of many ceramic matrix composites which plays a decisive role in controlling the fracture resistance of these materials (5).

3.4 .1 Interface Design Parameters

In order to achieve a tough ceramic composite, it is necessary to control the matrix-whisker/fiber interfacial properties and the fibers/whiskers must be evenly distributed throughout the matrix. In most cases, the interfacial bond must be weaker than either the whisker or the matrix since the whisker is often nearly as brittle as the matrix. A perspective regarding interfaces, classified either "strong" or "weak" is presented. A "strong" interface is characterized by

a relatively large Γ_i such that cracking of either the matrix or the fiber does not lead to interface debonding (Figure 13).

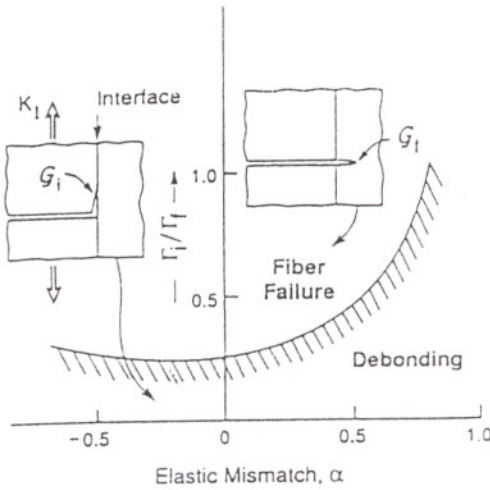


Figure 13. Debond characteristics for brittle matrix composites.

Conversely, a “weak” interface requirements in the presence of matrix-fiber cracks. Interfaces that debond are defined as “weak” but still exhibit a variety of behaviors within a composite, a reflected in the magnitude of τ .

The weak interface allows the crack to run along the interface or the whisker to slide out of matrix and the frictional forces to oppose further opening (bridging). The properties of interfaces in composites are characterized by two separate mechanical parameters: fracture energy Γ_i for debonding and an interfacial sliding resistance τ_i along debonding regions.

For debonding to initiate, the magnitude of Γ_i must be small. For brittle matrix system, in which matrix cracking typically precedes fiber cracking, debond initiation is governed by the ratio of Γ_i to the fiber fracture energy Γ_f . Debonding commences in preference to fiber failure provided that $\Gamma_i/\Gamma_f < 1/4$ (6). Since most ceramic fibers have a fracture energy of the order of $\Gamma_f = 20 \text{ J/m}^2$, an upper limit for $\Gamma_i \cong 5 \text{ J/m}^2$, which is broadly consistent with most experimental data. The low toughness interface is the first requirement to prevent fiber fracture during matrix crack growth (Figure 14).

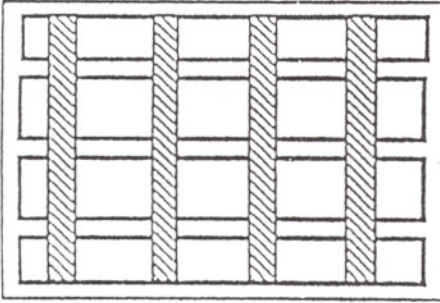


Figure 14. Matrix microcracking.

The coefficient of friction, μ , at the sliding interface plays a dominant role in ceramic composite toughening by determining the sliding resistance τ . Interfacial sliding resistance, τ_i , should be small enough to allow for a substantial pull-out contribution through frictional dissipation by encouraging fiber fracture at significant distances from the matrix crack plane(7). It is suggested that τ should be between 2 and 40 MPa and is given as,

$$\tau_i = \tau_0 \mu \sigma_{\perp} \quad (8)$$

where τ_0 is a constant term associated with roughness (most ceramic fibers exhibit some roughness at the nanometer scale), μ is a Coulomb friction coefficient and σ_{\perp} is the clamping stress normal to the interface. For a crack-bridging fiber, the bridging fraction is determined by the relative fiber-matrix displacements as controlled through the sliding resistance (8).

When a crack moves through a matrix containing fibers or whiskers, the following failure mechanisms may be expected to operate: matrix fracture, fiber-matrix interface debonding, fiber pull-out, etc. In conjunction with these mechanisms, fiber bridging, crack deflection and microcracking also take place

depending on the strength of constituents relative to that of interface. It is not necessary for all these failure mechanisms to operate simultaneously for a given system, and in some cases one of these toughness contributions may dominate the fracture toughness.

3.4.1.2 Fiber- Matrix Debonding

When the fiber fracture strain is greater than that of matrix ($\epsilon_f > \epsilon_m$), a crack originating at a point of stress concentration in the matrix is either halted by the fiber, if the local stress is not high enough, or it may pass around the fiber without destroying the interfacial bond. Figure 15 shows a propagating crack deflects along the interface rather than penetrates the fiber. Debond toughness value, R_d may be obtained by dividing the total strain energy stored in the fiber over the debond length l_d at its breaking stress σ_f^* by the nominal cross-section area of the composite:

$$R_d = \frac{V_f \sigma_f^* l_d}{2 \epsilon_f} \quad (5)$$

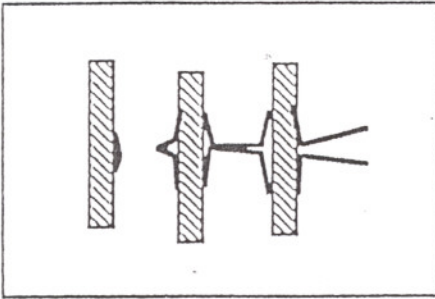


Figure 15. Schematic of fiber debonding.

3.4.1.3 Fiber Pull-Out

When propagates, crack pulls out the broken fibers from the matrix giving rise to a continuation of the post debonding frictional work (Figure 16).

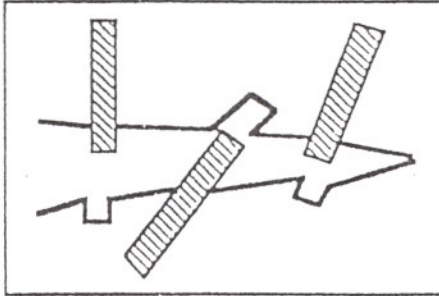


Figure 16. Schematic representation of fiber pull-out.

Based on the work done by the frictional shear stress τ_f which is assumed constant over a pull out distance l_{po} , the fiber pull-out toughness R_{po} is given by

$$R_{po} = \frac{2V_f \tau_f l_{po}^2}{d} \quad (5)$$

When the fiber length is less than the critical transfer length (i.e., $l < l_c$), all fibers are pulled out.

3.4.2 Interface Formation

There are two classical approach to the design of the fiber matrix interfacial zone in ceramic matrix composites. The first approach is through the *in-situ* formation of a weak interface resulting from chemical reactions at the fiber matrix interfaces during the high temperature step of composite processing. The interface in glass-ceramic matrix, $Li_2O-Al_2O_3-SiO_2$ (LAS).

reinforced with Nicalon-fibers, namely the Si-C-O ceramic grade fibers is produced by *in-situ* processing is given in Figure 17. Nicalon/glass ceramic composites are reactive systems in the temperature range corresponding to the hot pressing step, typically 1200-1400°C (8).

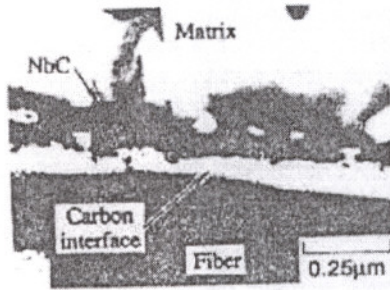


Figure 17. Transmission electron micrograph of the interfacial region of a lithium-alumino-silicate matrix and NicalonTM SiC fiber (8).

Chemical and structural analyses have shown that a complex multilayer fiber-matrix interfacial zone is formed *in-situ* as the result of an oxidation of the fiber surface by oxygen from the matrix. The key point is the presence of a thin carbon layer in the fiber matrix interfacial zone, which is often strongly textured and acts as mechanical fuse (low Γ_i and low to medium τ_i depending on the state of residual stresses, i.e. coefficient of thermal expansion mismatch). The second approach is based on the use of precoated fibers, the weak interface being deposited on the fiber surface prior to the deposition of the matrix itself. This second approach was extensively used for non-oxide composites, such as C/ SiC, SiC/SiC composites. Chemical vapor deposition (CVD) or chemical vapor infiltration (CVI) are the most commonly used techniques and solution/gel or sol/gel process and polymer pyrolysis technique are particularly appropriate for the deposition of simple, binary or ternary oxide interfaces. The interface is formed on the fiber surface through the repetition of dip coating/gelification/drying/firing sequences in sol/gel process. The other way to control adhesion is to coat the fibers with a thin layer of pyrolytic

carbon. An example of the presence of this carbon layer is given by Figure 18 (5).

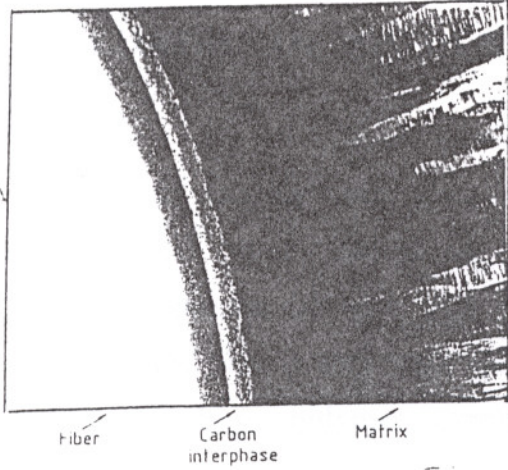


Figure 18. Transmission electron micrograph of the interfacial zone fiber-matrix in a SiC-SiC composite (5).

CHAPTER IV

COATING OF POWDERS

A number of chemical coating techniques can be used to prepare powders. These are chemical vapor deposition (CVD), chemical vapor infiltration (CVI), physical vapor deposition (PVD), molten-particle-deposition approaches (such as thermal and plasma spraying), electrophoretic coatings, ion implantation, glazing, enamelling, polymer pyrolysis, chemical solution techniques (precipitation, sol-gel technique, solvent evaporation and extraction) (22,23).

4.1 Chemical Solution Techniques

Chemical solution techniques provide high purity fine-sized powders. In this technique, suitable liquid solution containing the cations of interest is prepared first. A solid particulate phase may then be formed by precipitation or solvent evaporation or solvent extraction. Segregation is minimised by combining the ions in a precipitate or in a gel phase, or by extracting the solvent. The solid phase is usually a salt and can be decomposed without melting by calcination at relatively low temperatures. A porous friable calcine is then obtained in submicron size (22).

4.1.1 Chemical Precipitation Technique

Chemical precipitation technique can be used to prepare a variety of inorganic salts (Figure 19).

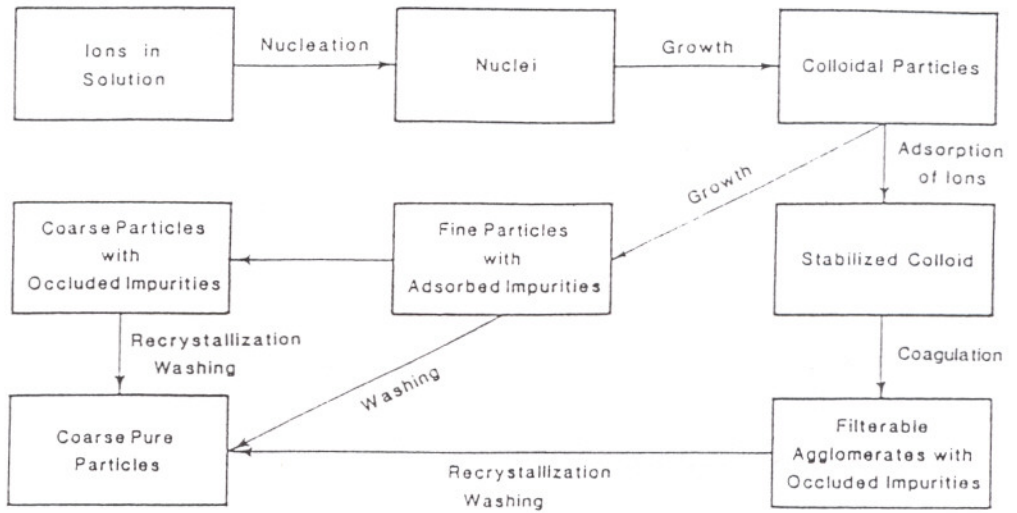


Figure 19. Processing flow diagram for the preparation of a pure precipitate.

The addition of a chemical precipitant to the solution or a change in temperature or pressure decreases the solubility limit and results in precipitation. Precipitation follows nucleation and growth stages. Impurity ions absorbed on the surfaces of particles may change precipitate growth rates in the solution. Relatively slow growth rates will cause an anisometric shape of precipitate particles. A higher degree of supersaturation may increase the nucleation rate and so produces a smaller particle size. The solution concentrations, pH, mixing and stirring rates and temperature are important variables controlling precipitation system. Precipitate may be purified by digestion, washing, or filtration. If the concentration of an ion in the salt differs from that in the solution, it is called heterogeneous precipitation. Suspension coating is a heterogeneous precipitation technique and homogeneous precipitation is avoided. In Figure 20 shows single component coating by direct heterogeneous precipitation. It is possible if reaction conditions are kept in the zone between the homogeneous and the heterogeneous nucleation limits.

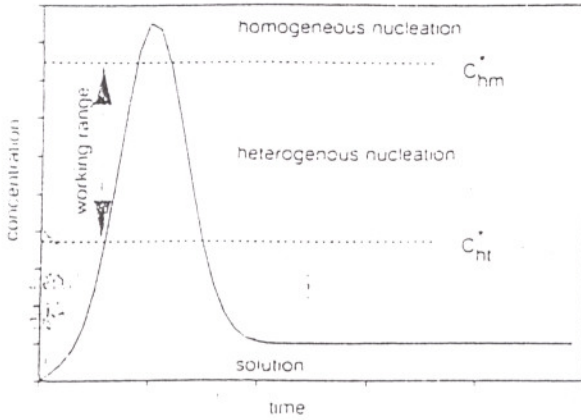


Figure 20. Single component coating powder by heterogeneous precipitation.

Multicomponent coating is shown in Figure 21. As the concentration of precipitate rises A will deposit in zone a, then AB would form in zone b. If the concentration rises further, to c, then A can precipitate homogeneously in the bulk solution, while AB is precipitating heterogeneously.

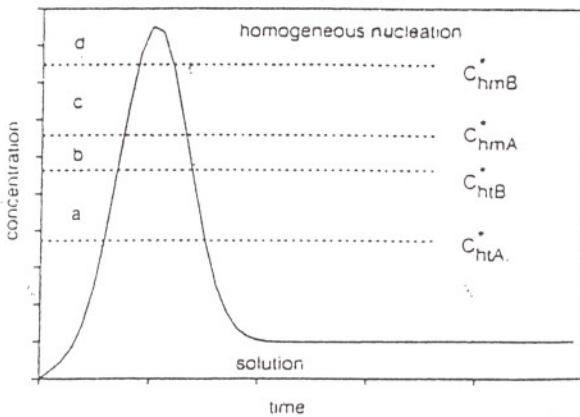


Figure 21. Multicomponent coating.

Precipitation techniques have been applied for preparing submicron size, high purity oxide powders. Particle sizes as small as 2 nm have been produced for some systems, and these have been used as commercial catalysts (14,22).

4.2 Coating of SiC Whiskers and Particulates with Al₂O₃

A number of techniques have been used to prepare powders by chemical methods such as hydrolysis of alkoxides, solvent removal etc. One successful method for producing an alumina powder precursor is the controlled precipitation of hydrated aluminium sulfate. Its ability to control the size, size distribution, degree of agglomeration and shape of the precipitates that makes these processes interesting. In 1984, Blendell et al (4) reported that high purity and high density alumina hydrate powders were precipitated from aluminium sulfate solution. They showed the solutions of aluminium sulfate containing urea yielded spherical, but varied in size from less than 1 to 5 μm . They reported that at higher excess of urea, many spherulitic precipitates were seen. It was suggested that the supersaturation was very high at these present regions. They reported that when the change in pH is rapid, the supersaturation at nucleation was much larger than that necessary to overcome the nucleation barrier. In contrast, if the pH changed slowly, the small random fluctuations in concentration caused nucleation locally. The particles lose weight due to water and SO_4^{2-} evolution during heating and an open structure resulted. They reported that the samples were calcined to 900⁰C before isopressing. Pressed samples were fired at 1550⁰C for densification. They found that it was not possible to directly sinter the precipitated aluminium sulfate hydrate powders to high density during the transformation from $\gamma\text{-Al}_2\text{O}_3$ to $\alpha\text{-Al}_2\text{O}_3$. The calcination of the precipitated powder was required before sintering to reduce large pores due to the vermicular structure that inhibit densification.

Precipitation techniques have been applied for preparing submicron size, high purity oxide powders. Particle sizes as small as 2 nm have been produced for some systems, and these have been used as commercial catalysts (14,22).

4.2 Coating of SiC Whiskers and Particulates with Al₂O₃

A number of techniques have been used to prepare powders by chemical methods such as hydrolysis of alkoxides, solvent removal etc. One successful method for producing an alumina powder precursor is the controlled precipitation of hydrated aluminium sulfate. Its ability to control the size, size distribution, degree of agglomeration and shape of the precipitates that makes these processes interesting. In 1984, Blendell et al (4) reported that high purity and high density alumina hydrate powders were precipitated from aluminium sulfate solution. They showed the solutions of aluminium sulfate containing urea yielded spherical, but varied in size from less than 1 to 5 μm . They reported that at higher excess of urea, many spherulitic precipitates were seen. It was suggested that the supersaturation was very high at these present regions. They reported that when the change in pH is rapid, the supersaturation at nucleation was much larger than that necessary to overcome the nucleation barrier. In contrast, if the pH changed slowly, the small random fluctuations in concentration caused nucleation locally. The particles lose weight due to water and SO_4^{2-} evolution during heating and an open structure resulted. They reported that the samples were calcined to 900⁰C before isopressing. Pressed samples were fired at 1550⁰C for densification. They found that it was not possible to directly sinter the precipitated aluminium sulfate hydrate powders to high density during the transformation from $\gamma\text{-Al}_2\text{O}_3$ to $\alpha\text{-Al}_2\text{O}_3$. The calcination of the precipitated powder was required before sintering to reduce large pores due to the vermicular structure that inhibit densification.

At the same year, Sack et al (25), studied with high purity spherical particles of hydrated aluminium sulfate that formed by a precipitation process utilizing the urea decomposition reaction. Particles were subjected to heat treatment at temperatures up to 1300⁰C. Samples were subsequently characterized by XRD, FTIR, mercury porosimetry, nitrogen gas adsorption. Differential thermal analysis (DTA) and Thermogravimetric analysis (TGA) were run on uncalcined samples from room temperature to 1400⁰C. In their study, uncalcined particles were shown to contain a significant amount of hydration water. This can be removed at low temperatures (below ~450⁰C) without pore formation. High specific surface areas developed at temperatures in the range 600⁰ to 900⁰C.

In 1990, Kapolnek and De Jonghe (14) studied on the preparation and use of alumina-coated SiC whiskers to produce a homogeneous ceramic composite. They developed this technique to coat sub-micron particles with relatively thick layers of the matrix precursor. They also reported that precipitation technique was more economical than the other techniques such as CVD, PVD... They found that too many precipitates were obtained by changing the concentration of solutions. Very thick coatings on the whiskers were produced in a second coating process and calcined whiskers. Kapolnek and Dejonghe (14) reported that in the production of whisker-dispersed ceramics, the use of matrix coated whisker was effective for the uniform dispersion of whiskers.

In 1992, Nakamura and Kato (18) studied on the aluminium hydrate-coated particles. The objective of their study was the improvement of chemical stability and dispersion nature of particles, and homogenous addition or mixing of second phase. They found that the crystallization of alumina hydrate have a remarkable effect on the morphology of composite particles. They found that at high pH value up to 8,6 amorphous alumina hydrate which coated SiC whiskers and particles separated from the SiCw and SiCp after crystallisation into pseudo-boehmite. At this study, it was important to stop the reaction before crystallisation of alumina hydrate occurs.

In 1995, Kato et al (15) prepared the SiC whisker-reinforced alumina ceramics by using alumina-coated whiskers. They also determined the mechanical strength of the composites. They found that the use of matrix-coated whiskers was effective in improving the dispersion of whiskers in the resulting composite and hence improving the mechanical properties.

4.3 Shrink-Fit Idea

Green ware contains between 25 and 50 volume percent porosity. The amount depends on the particle size, particle-size distribution, and forming method used. During the firing process, this porosity is removed; the volume firing shrinkage is equal to the pore volume eliminated. This firing shrinkage can be decreased by the addition of nonshrinking material to the mix. If firing is carried to complete densification, the fractional porosity is equal to the shrinkage taking place during firing. This commonly amounts to as much as 35 vol % volume shrinkage or 12 to 15 % linear shrinkage. It causes difficulty in maintaining close tolerances. However, the main difficulties are warping or distortion caused by different parts of the ware. Nonuniform shrinking can sometimes cause cracks to open.

Thermal stresses, microcracks and cavities that occur during the heating to high temperatures and cooling from these high temperatures in the production decrease the density of the composite. The thermal stresses are produced due to the differences of thermal expansion coefficients. For example, the thermal expansion coefficient of SiC whisker is almost half of the Al_2O_3 matrix material and for instance, this difference within the thermal expansion coefficients causes the pull stress in the matrix during the sintering. On the other hand, the haphazard distribution of whisker causes extraordinary extension of the particles in the sections where the density of whisker is less. The cavities that are stuck inside expanded particles and that can not shrink, are another cause that decreases the density of composite.

In order to prevent thermal stresses caused by the thermal expansion and microcracks, cavities within whisker and matrix are produced during sintering which is the final phase of composite production. During the condense, the filling of these cavities by the matrix is ensured (Shrink-fit idea) (Figure 22).

The coating of whisker surfaces with polymer and the burning of the polymer before densification temperature of the matrix is an example of the above mentioned process that will obtain an area for the matrix to expand within whisker matrix (2). The second approach is to coat dispersed phase with the matrix substance. When the second phase coated with the matrix substance are used as a raw material, it is expected that the agglomeration of dispersed phase in the matrix can be reduced and a more uniform dispersion can be obtained. Furthermore, in the case where the substance of the whiskers is different from that of the matrix, the pre-coating of the whiskers with the matrix substance provides the same properties for them as for the matrix substance. Thus the preparation of ceramic composites with the use of matrix-coated whisker is effective method in improving the dispersion of the second phase and hence improving the mechanical properties. The aim of this study is to prepare of coating the secondary phase surface of dense ceramic materials by the precipitation technique.

In order to reduce shrinkage stresses, it is used frozen solutions of soluble solids (e.g. sodium chloride glucose and polyvinyl alcohol) and miscible liquids (e.g. glacial acetic acid and pure acetyl acetone) as matrices for carbon fibers and also resins which cure with zero volume shrinkage or expansion are highly desirable for various practical applications such as high performance adhesives , coatings, precision castings , dental fillings , binders for solid propellants , etc. For shrinkage control in polymers especially epoxies and polyesters has been a subject of much continuing research (2,6,14,16).

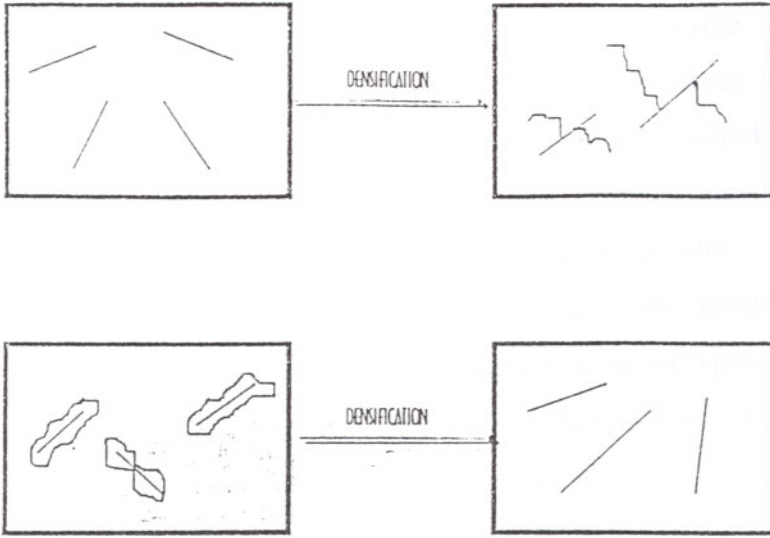


Figure 22. Shrink-fit idea.

CHAPTER V

EXPERIMENTAL WORK

In this study, the aim is to prepare and characterize alumina ceramic matrix composites reinforced with pre-coated SiC whiskers and particulates. The experimental study conducted in this work can be divided into three parts: coating of SiC whiskers and particulates and preparation and sintering of composites, and characterization of powders and composites.

In this work, the matrix phase in the composite samples was α -Al₂O₃ (Sumitomo AKP 50, >99.95% purity, particle size ~0.1 μ m). SiC used as a second phase in the form of whiskers were obtained from Tokai Carbon Ltd., and particulates were obtained from Alfa Company (α -SiC, 99.8% purity, 2 μ m). Al₂(SO₄)₃ (98% purity, MW= 342.15g/mol) and Urea (crystal, MW=60.06g/mol) were obtained from Aldrich Chemical Company, Inc.

5.1. Preparation of Coated SiC Whiskers and SiC Particulates

Controlled precipitation of hydrated aluminium sulfate from aqueous solutions was used for coating the second phase particles.

The experimental procedure used for the present study is schematically shown in Figure 23 for two different routes: SiC whisker and particulate coating. The coating process in SiC whisker route was started with the washing of whiskers with hydrogen fluoride (HF). This was done to remove the binder from the whisker preform provided from Tokai. After HF washing, distilled water was filtered several times over the whiskers in order to remove any acid remanent on whiskers' surfaces. Whiskers were then heated for several hours at 100°C to remove residual water. To conduct coating process, an aqueous solution containing 0,075 M Al₂(SO₄)₃ and 0.21M whisker or particulate were prepared. The solution was stirred with magnetic stirrer for 30 minutes to provide a good dispersion of whiskers or particulates. The suspension was then heated until 90 °C and at this point, Urea amounting 1.8M was added to the

solution. Urea was added to addition was to provide hydroxyl ions necessary and to avoid the development of regions of high pH in the solution. The solution was aged for 3 hours at 90 °C following Urea addition. The precipitation of hydrated basic aluminium sulfate occurred in this aging period. Throughout precipitation, the solution was vigorously stirred in order to prevent the whiskers from settling or agglomeration. The precipitation was stopped at pH = 5.5 for the reasons mentioned in Chapter IV. Subsequently, the coated whiskers or particulates were filtered from the solution and washed with distilled water. Finally, coated whiskers or particulates were dried in air before used in composite preparation step.

Differential thermal analysis (DTA) were run on uncalcined samples from room temperature to 1500⁰C in a static air atmosphere at a heating rate of 10⁰C/min, 5⁰C/min and 2⁰C/min using Shimadzu 50 DTA. Thermogravimetric analysis (TGA) up to 1000⁰C was carried out at 10⁰C/min, 5⁰C/min and 2⁰C/min rate on the uncalcined sample using Shimadzu 51 TGA. Percentage weight loss was also determined on samples. Infra-red spectra were determined using a Fourier Transform Infrared (FTIR) spectrometer. Samples were prepared by mixing with potassium bromide (0.5 wt % sample, 99.5 wt % KBr) and pressing into a disk shape in an 1.2 cm diameter steel die.

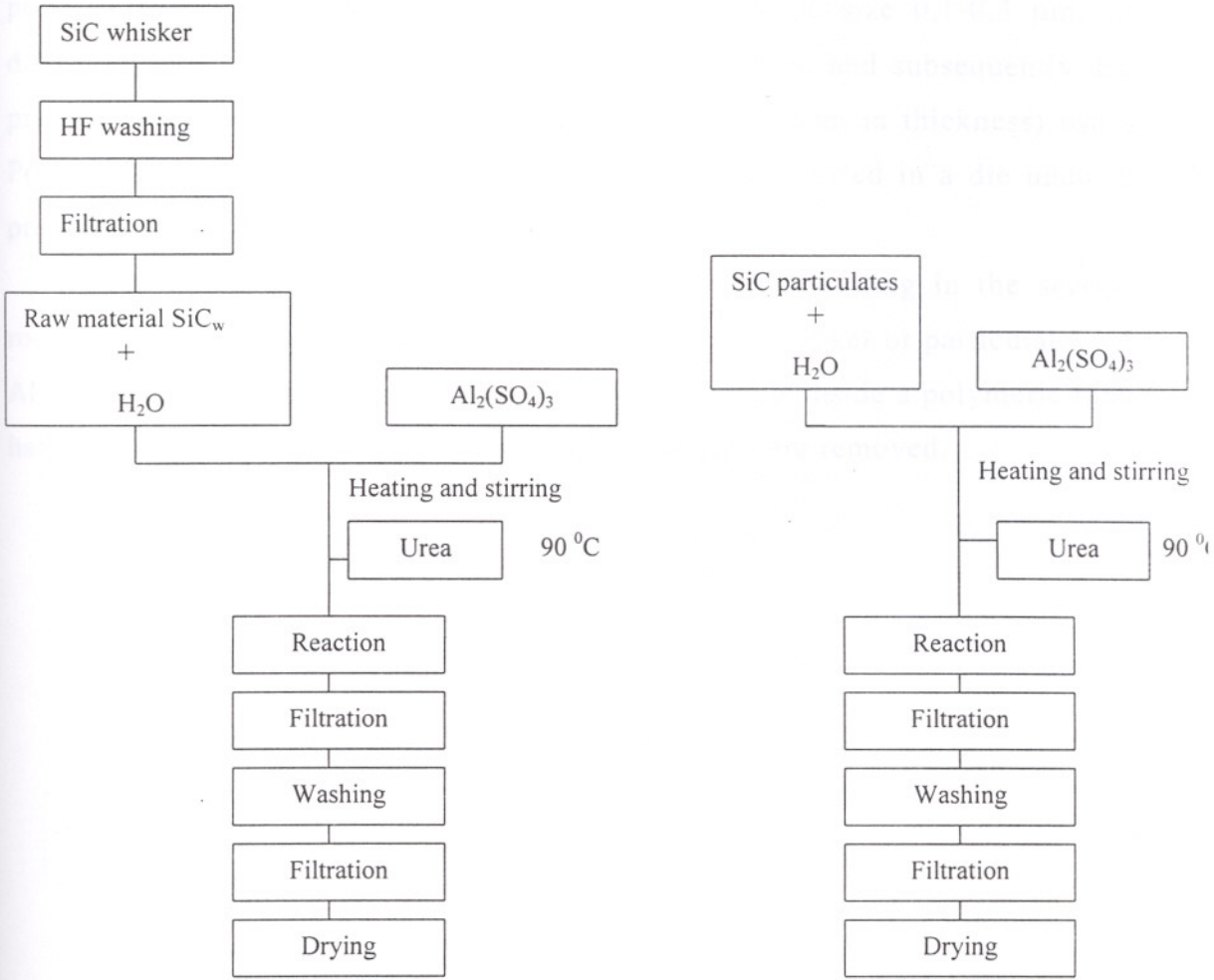


Figure 23 The preparation procedures for alumina hydrate-coated SiC whiskers and particulates

5.2. Composite Preparation and Consolidation

Two different composite preparation routes were used in this study: die pressing and slip casting (Figure 24). For both routes, alumina hydrate coated

and uncoated SiC whiskers and particulates were mixed with fine α -Al₂O₃ powders (Sumitomo AKP50, >99,99 % purity, particle size 0,1-0,3 μ m) in distilled water. In the first route, the mixture was dried and subsequently dry pressed into disc-shape compacts (10 mm diameter, 3 mm in thickness) using Poly Vinyl Alcohol (PVA) as binder. Pressing was achieved in a die under a pressure of 150 Bars.

The composite compacts were prepared by slip casting in the second route. Slips containing 45-60 volume fraction of SiC whisker or particulate and Al₂O₃ powders in were cast on the porous plaster molds inside a polymeric tube having 10-mm diameter. After drying, the compacts were removed.

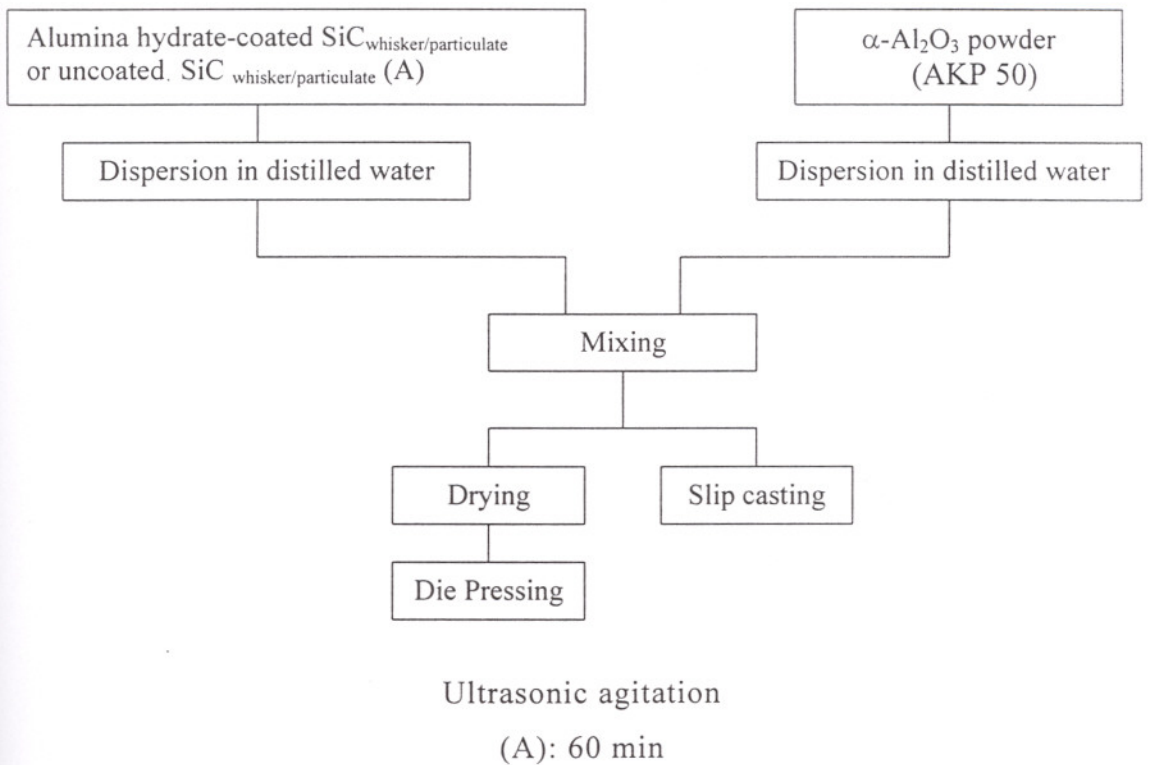


Figure 24 Preparation of alumina hydrate-coated SiC whiskers and particulates-Al₂O₃ Composites

The green compacts produced were finally sintered at 1450⁰C for 2 hours. Density of SiC whiskers-Al₂O₃ and SiC particulates-Al₂O₃ composites were measured by Archimedes principle using the density kit (Sartorius YDK 01 balance).

5.3 Sample Preparation of the Microhardness Test

In this study microhardness test measurements of the 6 different specimen, sintered Al₂O₃-%20 uncoated SiCp, Al₂O₃-%20 coated SiCp, Al₂O₃-%30 coated SiCp, Al₂O₃-%20 coated SiCw, Al₂O₃-%40 coated SiCw were performed with the time testing instruments HV 1000 vickers microhardness tester. Before the hardness test, each specimen surface were prepared for mechanical testing by the following procedure shown in Figure 25.

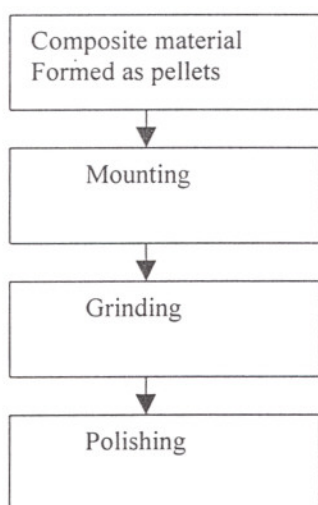


Figure 25 Schematic representation of sample preparation of microhardness test

Samples were mounted inside a polymeric material to obtain a uniform level. This is also important for the optical microscope observations. Buehler

simplement 2 mounting press device was used for the mounting process. After mounting, grinding process is necessary to reduce the amount of deformation brought about by the mounting process. Samples were grinded by using Metaserv 2000 grinder with grinding papers with 600 grit size and then 1000 grid size at 400 n/Min speed. Polishing is for the grinding scratches and heavily deformed layer brought about by the grinding process 1 μ m and 6 μ m abrasive particles were used for mechanical polishing of composites.

CHAPTER VI

RESULTS AND DISSCUSION

6.1 Preparation of Alumina Hydrate-Coated SiC Whiskers and SiC Particulates.

Aluminium sulfate was the most suitable aluminium salt as stated in the literature for preparing alumina hydrate coated SiC particles under experimental conditions [SiC_{w/p}]= 0,21M, [Al₂(SO₄)₃] =0.075M, [Urea]=1.8M and reaction temperature $\cong 90^{\circ}\text{C}$.

The change of pH uniformly through out the solution allows fast reaction and yields spheres. Urea has been used for providing a supply of hydroxyl ions necessary for the precipitation reaction. Upon heating, urea decomposes slowly producing CO₂ and NH₄⁺ ions above 90⁰C. As the pH of the solution is increased by the urea decomposition, the solubility limit decreases. But precipitation does not occur until the concentration of aluminium sulfate hydrate is above the solubility limit. Rapid nucleation then appears. Growth of the nucleated particles occurs until no further nucleation occurs. Thus all the particles are of the same size. The particle shape is spherical rather than faceted due to the presence of the SO₄²⁻ (Figure26). Formamide can also be used as a precipitating agent (4). As the pH became higher spherical particles deposited on silicon carbide whiskers or the particulates.

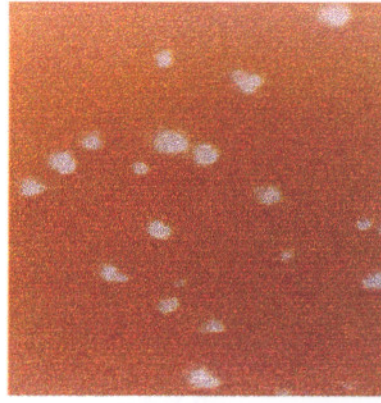
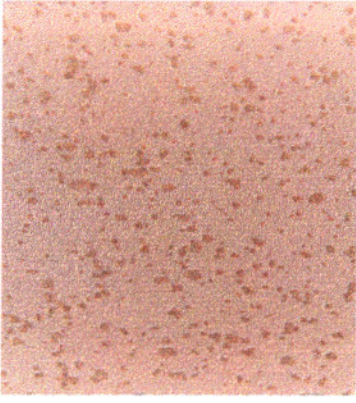


Figure 26. Aluminium sulfate hydrate spherical particles.

The optical micrograph and SEM pictures of uncoated SiC particulates and whiskers are shown in Figures 27 and 29. When the precipitation starts as the decomposition of urea, the aluminium sulfate hydrate is deposited on the SiC. The coated particulates and whiskers are heavily agglomerated at lower phase values (3-4) and the system becomes dispersed at higher pH values ($\text{pH} > 5.5$).

The morphology of the coated particles are shown in Figures 28 and 30. In the first sample ($\text{pH} = 3.36$), particles are heavily agglomerated but still individual particles could be seen. The particle size of the precipitate increase with the increasing pH. These particles coagulated heavily around $\text{pH} = 4$. Particles were separated from each other above $\text{pH} = 5.5$. The variation of pH with time is shown in Figure 31 for SiC particulates. A similar curve was obtained by Nakamura and Kato (18).

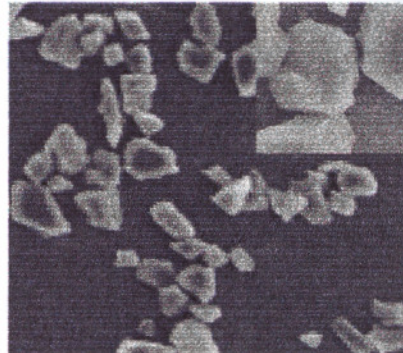
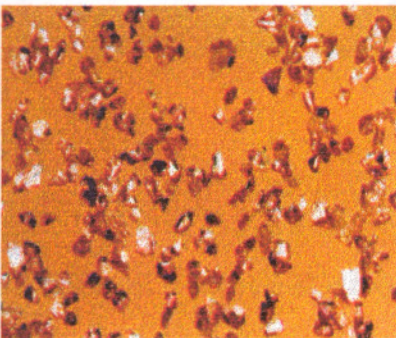
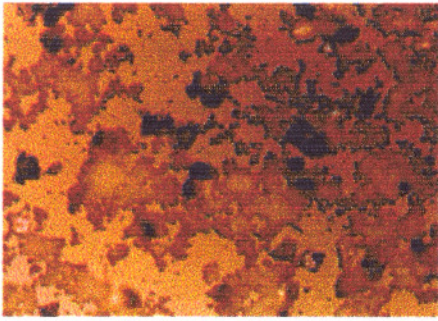
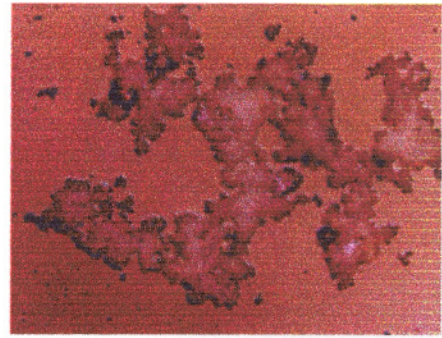


Figure 27 Reflected optical micrograph and Scanning Electron Micrograph of uncoated SiC particulates (particle size $\sim 20\mu\text{m}$).



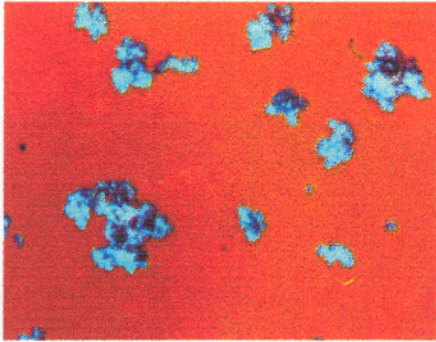
pH=3.36

20µm



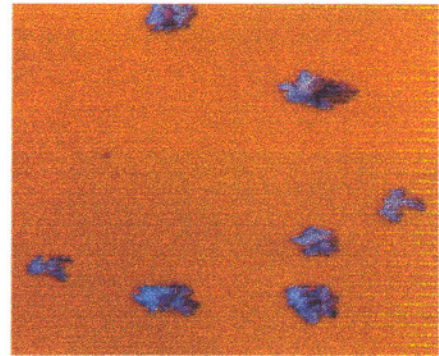
pH=4.05

20µm



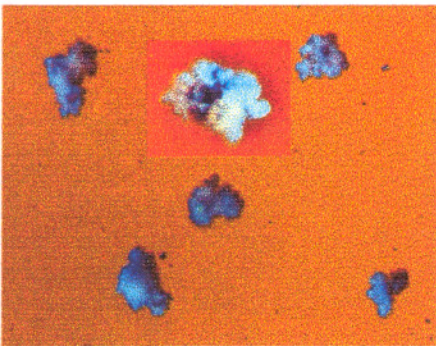
pH=5.1

20µm



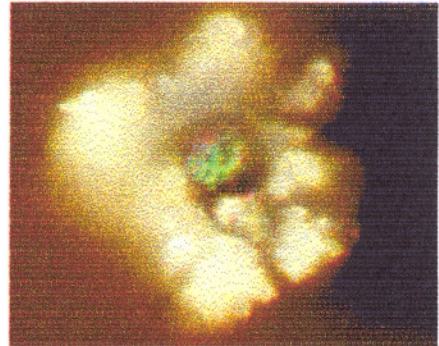
pH=5.5

20µm



pH=6.1

20µm



pH=6.47

20µm

Figure 28. Reflected optical micrographs of the morphology of coated SiC particulates at different pH values.

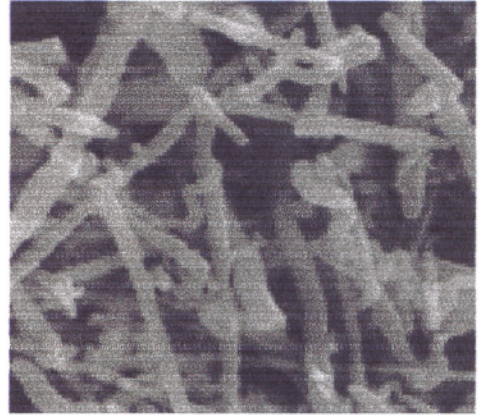
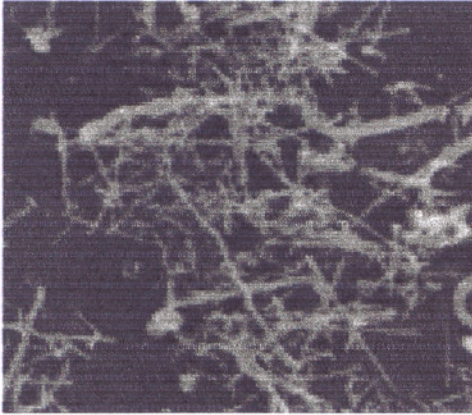
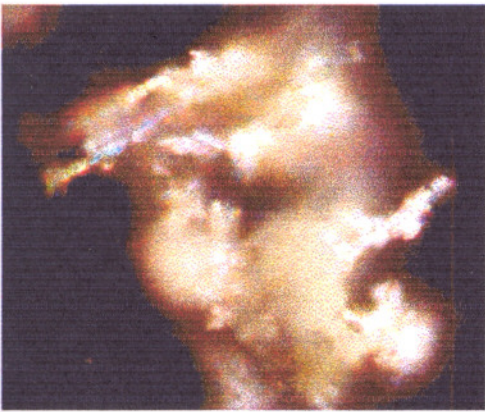
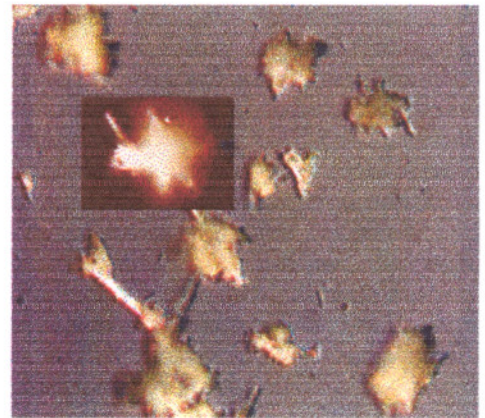


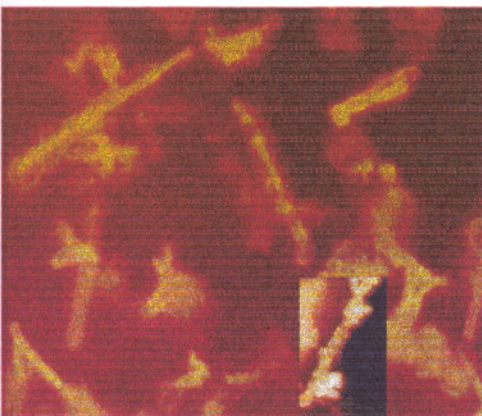
Figure 29 Scanning Electron Micrographs of uncoated SiC whiskers



pH=3.65

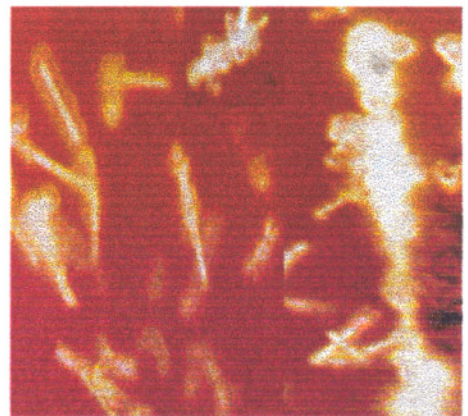


pH=4.3



pH=5.5

10 μ m



pH=6.8

10 μ m

Figure 30. Reflected optical micrographs of alumina hydrate coated SiC whiskers at different pH values.

At higher excess of urea, many spherical particles were seen. This may indicate the presence of locally very high supersaturation. In addition, at high concentrations of aluminium sulfate, the spherical shape and uniformity of size were not preserved, too.

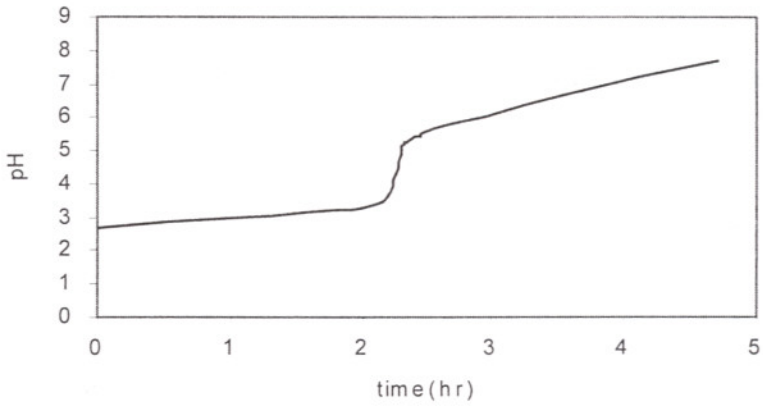


Figure 31. pH curve for SiC particulates.

The morphology of the precipitates changed with final pH. When the reaction was stopped at pH=7.2, the alumina hydrate yielded surrounding SiC particulates and whiskers as shown in Figures 32 and 33, respectively .

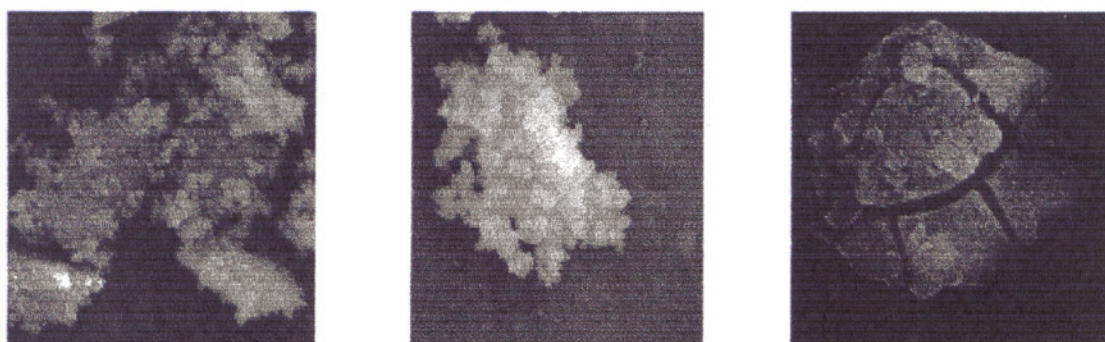


Figure 32. Scanning electron micrographs of alumina hydrate coated SiCp.

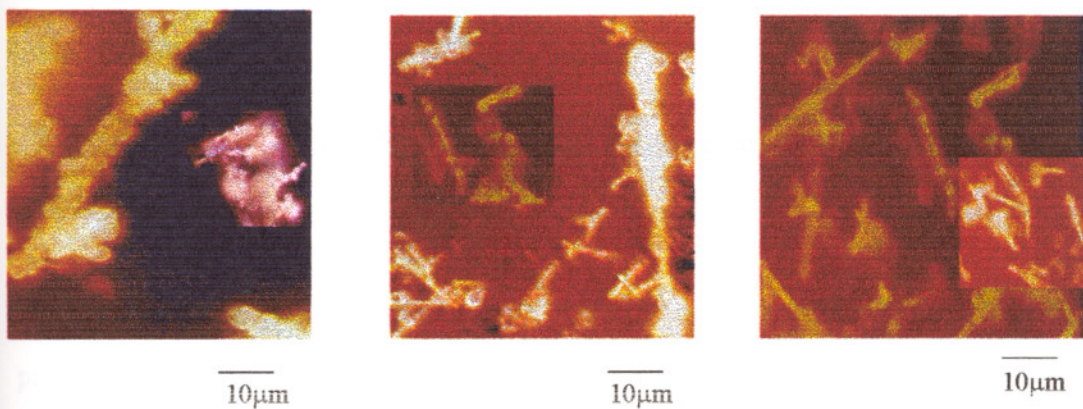


Figure 33. Reflected optical micrographs of Alumina Hydrate-coated SiC whiskers.

The XRD pattern in Figure 34 shows that the coating of the uncalcined sample at pH=6.47 is amorphous.

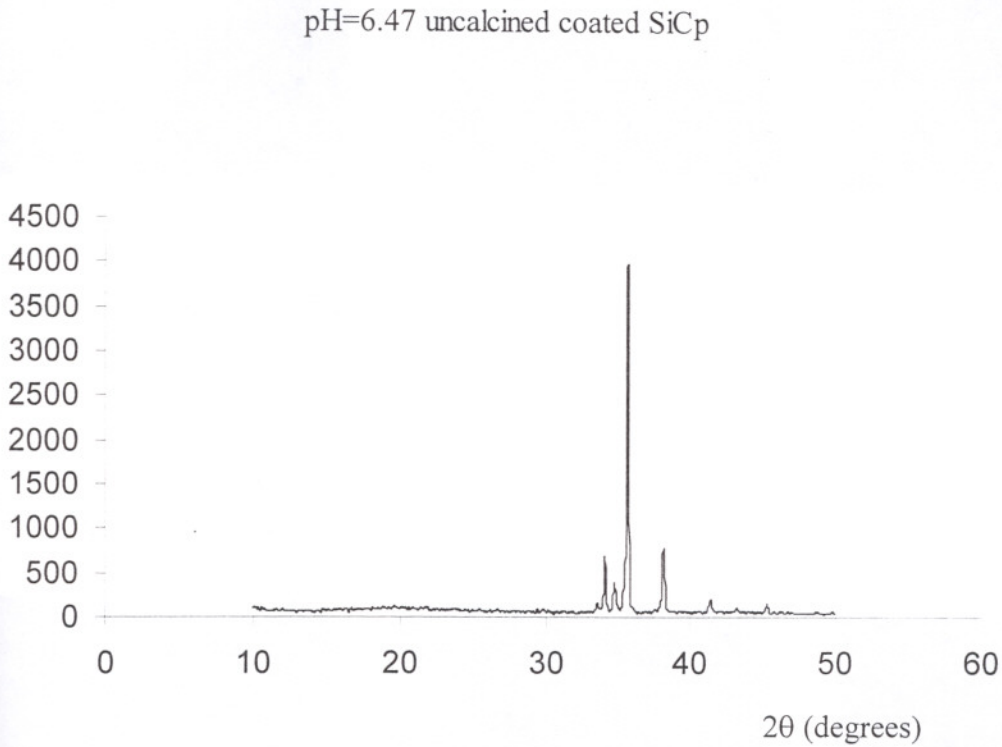


Figure 34. X-Ray Diffraction pattern for coated SiC particulates.

The only phase observed in XRD for uncalcined samples is SiC particulates. This indicates that a considerable amount of amorphous material is still present on the SiC particulates. On the other hand, when the reaction was continued up to pH=8.6; the alumina hydrate on the SiC whiskers and SiC particulates crystallized into pseudo boehmite as shown in Figure 35 and Figure 36, respectively as reported (18).

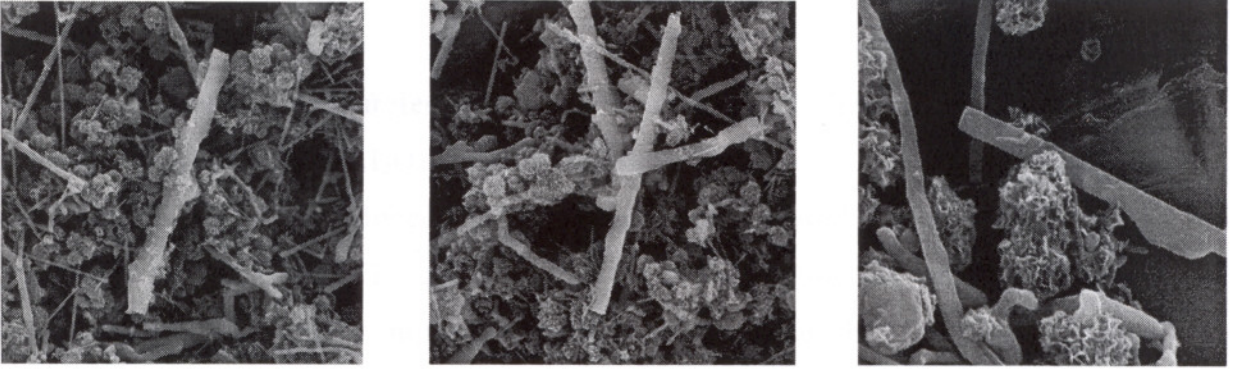


Figure 35. Scanning electron micrographs of coated SiCw at $\text{pH} > 8.6$.

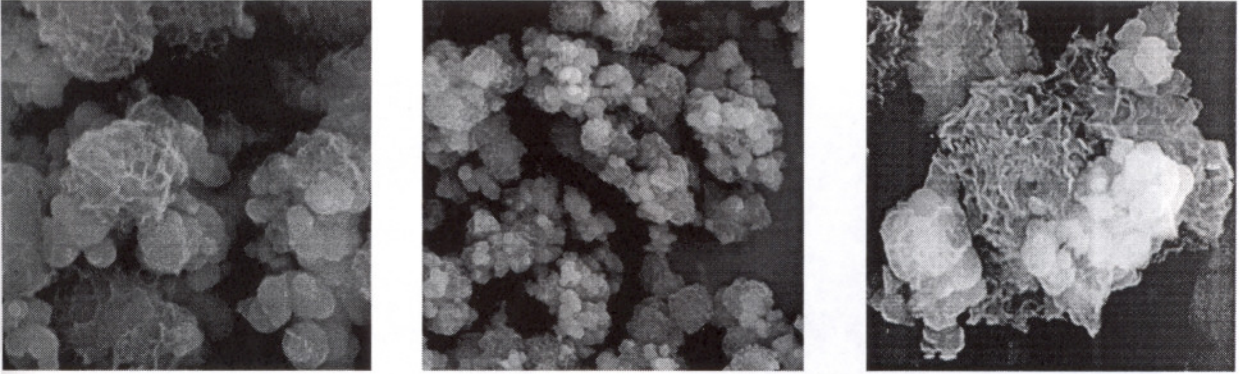


Figure 36. Scanning electron micrographs of SiCp at $\text{pH} > 8.6$.

The amorphous $\text{Al-SO}_4\text{-OH}$ coating at $\text{pH}=6.47$ separated from the surface of SiC whiskers and particulates after crystallization into pseudo boehmite at $\text{pH}=8.7$ shown in Figure 35 and 36. In order to prevent the destruction of the composite structure, it is important to stop the reaction before crystallization of alumina hydrate occurs.

6.2 Effect of SiC whisker on Densification

Typically, pressureless sintering to >95 % of theoretical density can produce high density Al_2O_3 without whiskers. Figure 37 shows the fracture surface of $\alpha\text{-Al}_2\text{O}_3$ produced by firing die-pressed $\alpha\text{-Al}_2\text{O}_3$ used as the matrix material in this study. The grain size of the sintered alumina was measured as 3-4 μm . SiC prevents complete densification because they are inert during sintering. The thermal expansion coefficient of SiC whisker is almost half of the alumina matrix. Between 20 $^\circ$ and 1000 $^\circ\text{C}$, $\alpha_{\text{SiC}}=4.8 \cdot 10^{-6} \text{ C}^{-1}$ and $\alpha_{\text{alumina}}=8.5 \cdot 10^{-6} \text{ C}^{-1}$ (27). This difference between the thermal expansion coefficients causes the pull stress in the matrix during the sintering. SiC whiskers interfere with the shrinkage of the matrix. This is the most important reason of low density of whisker composites. The irregular distribution of the reinforcement causes the formation of large pores.

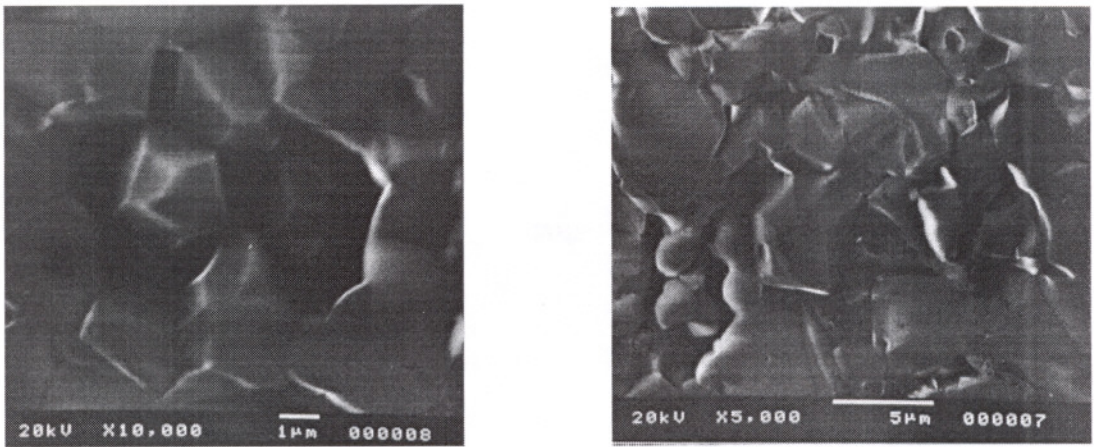


Figure 37. Fracture surface of Al_2O_3 produced by die-pressed and sintered at 1450 2h.

In order to prevent thermal stresses caused by thermal expansion coefficient mismatch between the matrix and second phase and microcracks and large pores, the whiskers and particulates were coated with $\text{Al-SO}_4\text{-OH}$ precursor. Upon heating the precursor transformed to $\alpha\text{-Al}_2\text{O}_3$ by providing empty spaces for matrix densification during sintering.

Fracture surfaces of composites pressureless sintered containing 20 vol.% SiC whiskers and particulates are shown in Figure 38 and 39, respectively. The large holes observed in these picture most likely represent the whisker and particulate removals. Large holes are evidences of agglomeration of whiskers and particulates. Similar results were obtained by Smith et al (27).

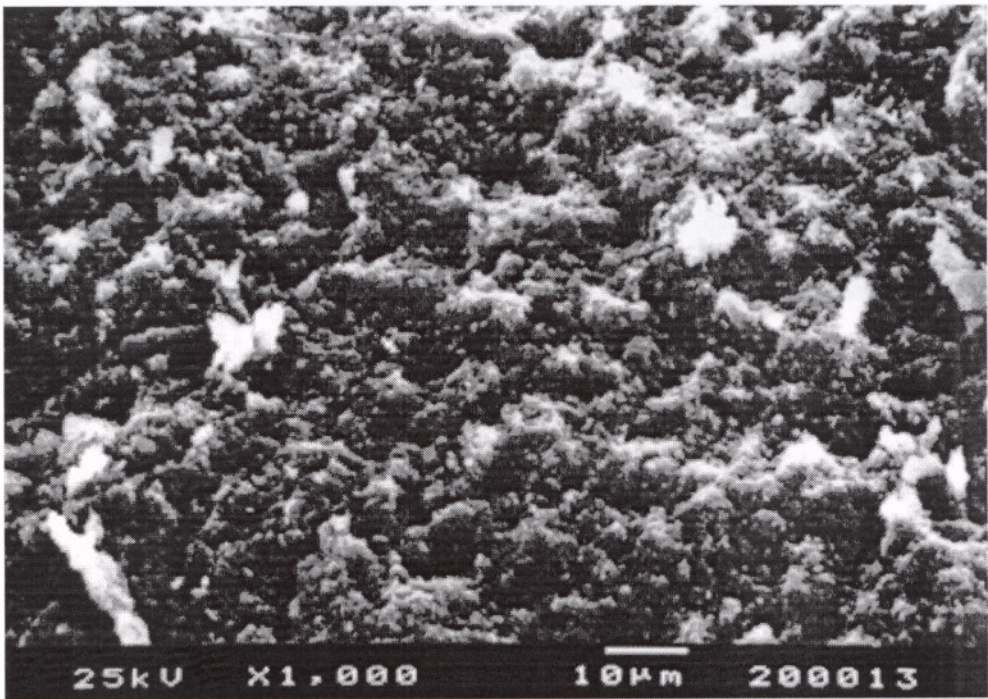


Figure 38. Scanning electron micrograph of fracture surface of
20vol%SiC_w-Al₂O₃.

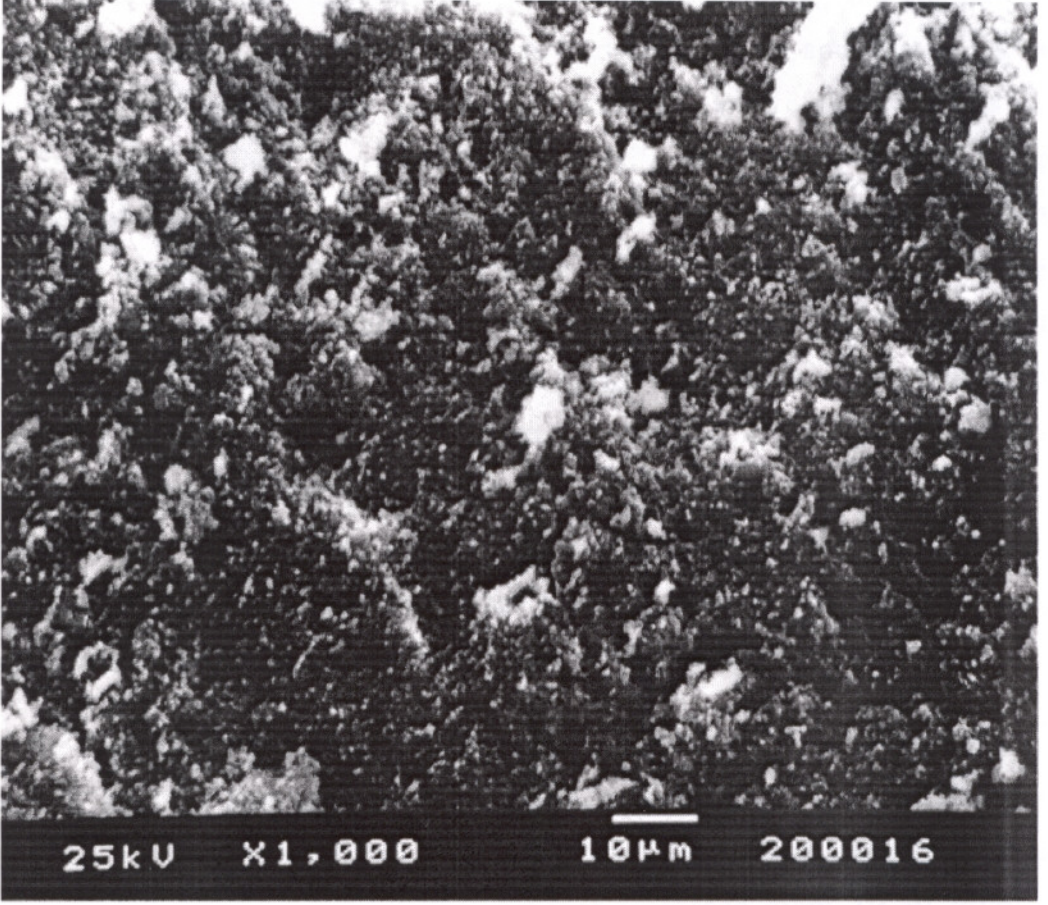


Figure 39. Scanning electron micrograph of fracture surface of 20 vol.%
SiCp-Al₂O₃.

6.3 Density Measurements

Pressureless sintering of ceramic composites containing whiskers is a difficult challenge. The whiskers interfere with powder mixing and compaction by forming bridges. This prevents uniform particle packing and thus complete densification during sintering. Unlike hot pressing, where the whiskers are forced to rearrange their positions during densification, there is no external force available to assist whisker rearrangement in pressureless sintering. The difficulty of pressureless sintering whisker reinforced composites was reported Tieg et al (3,12). Al_2O_3 containing 15 vol.% SiC whiskers could be sintered to only 80% of theoretical density, whereas material of the same composition could be hot pressed to over 98 % of theoretical density (30,31). Fully dense alumina/silicon carbide composites are normally obtained by hot pressing at $T \cong 1850^\circ\text{C}$. The hot pressing causes the whiskers to be oriented with their length randomly perpendicular to the hot pressing axis. Hot pressing preferred orientation leads to anisotropy in both fracture toughness and strength (9).

The density of composites containing from 10 to 40% both uncoated and coated SiC whisker and particulate are given in Tables 1-6. The calculation of the density of these composites is given in Appendix. The density of these composites decreased as the whisker content increased from 10-40 %vol as shown in Figures 40-43. The decreasing density of both particulates and whiskers composites were attributed to the increasing of reinforcement phase content and large pores caused by thermal expansion coefficient mismatch between the matrix and reinforcement phase and also hard agglomerated SiC whiskers and particulates. The particulate composites have higher density compared to the whisker composites, which are prepared in the same volume content. The reason of low density in the whisker composites was discussed before.

The composites prepared with 1100°C calcined-coated SiC particulates and whiskers have slightly high density than the uncalcined composites. The density of these samples and the effect calcined coated SiC particulates and

whiskers on densification of Al_2O_3 matrix composite are shown in Tables 5 and 6 and Figures 44 and 45, respectively.

The density of both uncoated SiC whiskers and particulates are significantly low compared with the literature. This may be due to the irregular distribution of second phase in the matrix. The coated SiC whisker- Al_2O_3 and coated SiC particulate- Al_2O_3 composite have higher density than the uncoated SiC whisker- Al_2O_3 and uncoated SiC particulate- Al_2O_3 composites. The reason behind this relative increase in density between the coated-uncoated whisker/particulate composites was not very clear. This increase may partially be due to shrink-fit idea or the formation of a better dispersion during the preparation of the powder mixture.

Table 1. Effect of uncoated SiC particulates on sintering.

| Sample No | Green Density g/cm ³ | Dg (mm) | hg (mm) | Wg (g) | Wd (g) | Ws (g) | Wss (g) | Sintered Density g/cm ³ | thd% |
|-----------|---------------------------------|---------|---------|--------|--------|--------|---------|------------------------------------|-------|
| UP1(1) | 1.94 | 14.12 | 3.55 | 1.1175 | 1.1013 | 1.1665 | 0.743 | 2.59 | 66.34 |
| UP1(2) | 1.95 | 14.07 | 3.58 | 1.1169 | 1.1086 | 1.1778 | 0.757 | 2.62 | 67.11 |
| UP1(3) | 1.95 | 14.16 | 3.57 | 1.1175 | 1.1063 | 1.1644 | 0.751 | 2.67 | 68.4 |
| UP1(4) | 1.98 | 14.1 | 3.58 | 1.1236 | 1.1178 | 1.1877 | 0.759 | 2.6 | 66.6 |
| UP1(5) | 1.96 | 14.14 | 3.62 | 1.1284 | 1.1186 | 1.1804 | 0.756 | 2.63 | 67.37 |
| UP2(1) | 1.91 | 14.08 | 3.62 | 1.0912 | 1.0813 | 1.1619 | 0.743 | 2.57 | 67.14 |
| UP2(2) | 1.93 | 14.1 | 3.53 | 1.11 | 1.0935 | 1.1675 | 0.75 | 2.6 | 67.93 |
| UP2(3) | 1.92 | 14.08 | 3.52 | 1.1108 | 1.0935 | 1.1598 | 0.75 | 2.66 | 69.49 |
| UP2(4) | 1.91 | 14.08 | 3.68 | 1.1488 | 1.1306 | 1.211 | 0.778 | 2.6 | 67.93 |
| UP2(5) | 1.94 | 14.11 | 3.62 | 1.1233 | 1.1133 | 1.202 | 0.759 | 2.5 | 65.32 |
| UP2(6) | 1.92 | 14.08 | 3.63 | 1.0947 | 1.0899 | 1.1698 | 0.748 | 2.57 | 67.14 |
| UP3(1) | 1.87 | 14.11 | 3.58 | 1.0509 | 1.0487 | 1.1567 | 0.736 | 2.48 | 66.11 |
| UP3(2) | 1.9 | 14.08 | 3.53 | 1.0595 | 1.0442 | 1.1434 | 0.729 | 2.51 | 66.91 |
| UP3(3) | 1.88 | 14.12 | 3.59 | 1.0691 | 1.0596 | 1.1589 | 0.745 | 2.55 | 67.98 |
| UP3(4) | 1.9 | 14.11 | 3.52 | 1.0639 | 1.059 | 1.1753 | 0.747 | 2.46 | 65.58 |
| UP3(5) | 1.87 | 14.09 | 3.59 | 1.0581 | 1.0443 | 1.1587 | 0.74 | 2.48 | 66.11 |
| UP4(1) | 1.81 | 14.1 | 3.76 | 1.0656 | 1.0545 | 1.2042 | 0.765 | 2.39 | 65.03 |
| UP4(2) | 1.84 | 14.06 | 3.62 | 1.0356 | 1.0247 | 1.1676 | 0.743 | 2.4 | 65.03 |
| UP4(3) | 1.8 | 14.1 | 3.65 | 1.0297 | 1.018 | 1.1649 | 0.738 | 2.37 | 64.5 |
| UP4(4) | 1.78 | 14.06 | 3.68 | 1.0213 | 1.0196 | 1.1628 | 0.739 | 2.397 | 65.22 |
| UP4(5) | 1.78 | 14.1 | 3.75 | 1.0453 | 1.0326 | 1.1755 | 0.748 | 2.4 | 65.3 |

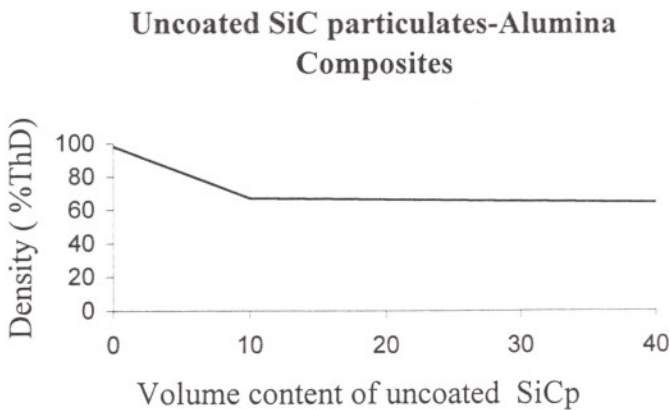


Figure 40. Effect of uncoated SiCp on densification of Alumina matrix composites.

Table 2. Effect of coated SiC particulates on sintering.

| Sample No | Green density g/cm ³ | Dg (mm) | hg (mm) | Wd (g) | Wg (g) | Ws (g) | Wss (g) | interd Density g/cm ³ | %thd |
|-----------|---------------------------------|---------|---------|--------|--------|--------|---------|----------------------------------|-------|
| CP1(1) | 2.3 | 14.12 | 2.74 | 0.982 | 1.001 | 1.029 | 0.712 | 3.09 | 79 |
| CP1(2) | 2.32 | 14.12 | 2.84 | 1.034 | 1.039 | 1.084 | 0.754 | 3.12 | 80 |
| CP1(3) | 2.35 | 14.05 | 2.89 | 1.018 | 1.038 | 1.066 | 0.738 | 3.16 | 81 |
| CP1(4) | 2.32 | 14.15 | 2.81 | 1.008 | 1.028 | 1.051 | 0.733 | 3.15 | 81 |
| CP1(5) | 2.34 | 14.15 | 2.73 | 1.022 | 1.041 | 1.07 | 0.741 | 3.1 | 80 |
| CP2(1) | 2.24 | 14.18 | 2.88 | 1.014 | 1.029 | 1.087 | 0.722 | 2.77 | 72 |
| CP2(2) | 2.26 | 14.2 | 2.95 | 1.025 | 1.06 | 1.094 | 0.727 | 2.78 | 73 |
| CP2(3) | 2.35 | 14.17 | 2.86 | 1.054 | 1.06 | 1.119 | 0.748 | 2.83 | 74 |
| CP2(4) | 2.55 | 14.16 | 2.91 | 1.055 | 1.062 | 1.126 | 0.75 | 2.8 | 73 |
| CP3(1) | 2.3 | 14.21 | 2.81 | 1.025 | 1.028 | 1.098 | 0.712 | 2.64 | 71 |
| CP3(2) | 2.22 | 14.17 | 2.9 | 1.016 | 1.019 | 1.086 | 0.703 | 2.62 | 70 |
| CP3(3) | 2.14 | 14.21 | 2.97 | 1.029 | 1.018 | 1.084 | 0.699 | 2.61 | 70 |
| CP3(4) | 2.24 | 14.19 | 2.85 | 1.004 | 1.015 | 1.072 | 0.693 | 2.63 | 70 |
| CP3(5) | 2.11 | 14.23 | 3.01 | 1.011 | 1.02 | 1.083 | 0.698 | 2.61 | 70 |
| CP3(6) | 2.22 | 14.21 | 2.86 | 1.006 | 1.014 | 1.078 | 0.696 | 2.63 | 70 |
| CP4(1) | 2.12 | 14.12 | 2.98 | 1.015 | 1.01 | 1.197 | 0.741 | 2.4 | 65.3 |
| CP4(2) | 2.06 | 14.17 | 2.88 | 0.994 | 0.99 | 1.155 | 0.715 | 2.39 | 65.03 |

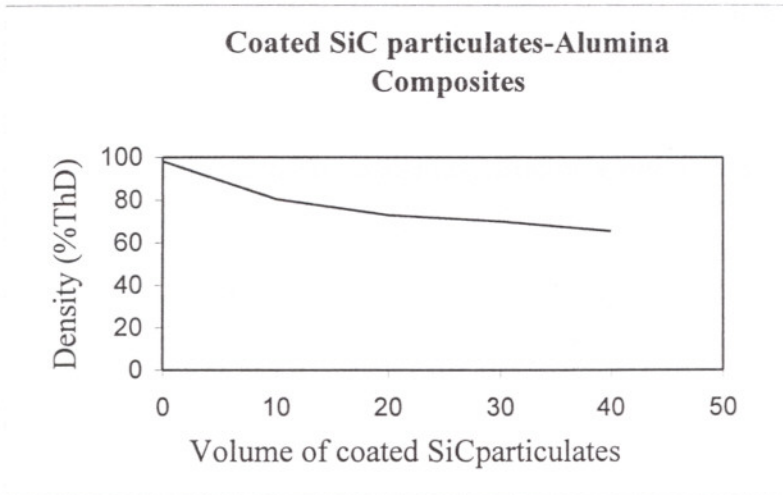


Figure 41. Effect of coated SiC particulates on densification of Alumina matrix composites.

Table 3. Effect of uncoated SiC whiskers on sintering.

| Sample No | Green Density g/cm ³ | Dg (mm) | hg (mm) | Wg (g) | Wd (g) | Ws (g) | Wss (g) | Sintered density g/cm ³ | %thd |
|-----------|---------------------------------|---------|---------|--------|--------|--------|---------|------------------------------------|------|
| UW1(1) | 2.14 | 4.27 | 3 | 1.0312 | 1.0444 | 1.0217 | 0.699 | 2.47 | 67 |
| UW1(2) | 2.16 | 14.28 | 2.96 | 1.0451 | 1.0308 | 1.102 | 0.6906 | 2.5 | 68 |
| UW1(3) | 2.17 | 14.27 | 3.07 | 1.0655 | 1.0509 | 1.1301 | 0.7035 | 2.46 | 67 |
| UW1(4) | 2.12 | 14.25 | 2.78 | 0.9473 | 0.8763 | 0.9438 | 0.593 | 2.52 | 69 |
| UW2(1) | 1.6 | 14.28 | 3.98 | 1.0597 | 1.0436 | 1.1888 | 0.7243 | 2.25 | 60 |
| UW2(2) | 1.62 | 14.27 | 3.97 | 1.0536 | 1.0475 | 1.1924 | 0.7256 | 2.25 | 60 |
| UW2(3) | 1.62 | 14.28 | 3.96 | 1.0549 | 1.0497 | 1.1911 | 0.7258 | 2.26 | 60 |
| UW2(4) | 1.62 | 14.29 | 3.92 | 1.0589 | 1.0441 | 1.185 | 0.7208 | 2.25 | 60 |
| UW3(1) | 1.62 | 14.22 | 4.06 | 1.0522 | 1.0475 | 1.1897 | 0.7417 | 2.29 | 60 |
| UW3(2) | 1.64 | 14.19 | 3.92 | 1.0237 | 1.0194 | 1.198 | 0.729 | 2.25 | 59 |
| UW3(3) | 1.65 | 14.25 | 3.86 | 1.0285 | 1.0261 | 1.1801 | 0.7241 | 2.25 | 59 |
| UW3(4) | 1.67 | 14.26 | 3.91 | 1.0487 | 1.0036 | 1.1876 | 0.731 | 2.28 | 60 |
| UW3(5) | 1.63 | 14.23 | 3.88 | 1.0233 | 1.0296 | 1.1803 | 0.7302 | 2.29 | 60 |
| UW3(6) | 1.65 | 14.23 | 3.94 | 1.0434 | 1.0385 | 1.1739 | 0.7322 | 2.35 | 60 |
| UW4(1) | 1.69 | 14.14 | 3.82 | 1.0147 | 0.9999 | 1.1724 | 0.7181 | 2.2 | 57 |
| UW4(2) | 1.68 | 14.23 | 3.77 | 1.0076 | 0.9904 | 1.169 | 0.7225 | 2.23 | 57 |
| UW4(3) | 1.7 | 14.13 | 3.73 | 1.0266 | 1.0121 | 1.179 | 0.7332 | 2.27 | 59 |
| UW4(4) | 1.73 | 14.19 | 3.75 | 1.0257 | 1.0094 | 1.183 | 0.7303 | 2.23 | 57 |
| UW4(5) | 1.723 | 14.15 | 3.88 | 1.0513 | 1.0346 | 1.2171 | 0.7458 | 2.2 | 57 |

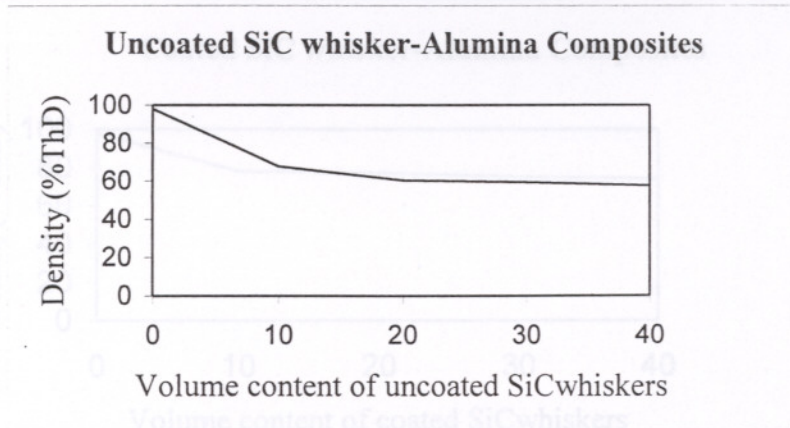


Figure 42. Effect of uncoated SiC whiskers on densification of the Alumina matrix composites.

Table 4. Effect of coated SiC whisker on sintering.

| Sample No | Green Density g/cm ³ | Dg (mm) | hg (mm) | Wg (g) | Wd (g) | Ws (g) | Wss (g) | Sintered density g/cm ³ | thd% |
|-----------|---------------------------------|---------|---------|--------|--------|--------|---------|------------------------------------|------|
| CW1(1) | 2,17 | 14,29 | 2,88 | 1,0042 | 0,9906 | 1,0222 | 0,6738 | 2,83 | 76 |
| CW1(2) | 2,26 | 14,28 | 2,85 | 1,034 | 1,0209 | 1,053 | 0,7036 | 2,91 | 78 |
| CW1(3) | 2,28 | 14,21 | 2,8 | 1,0108 | 0,9993 | 1,027 | 0,689 | 2,94 | 79 |
| CW1(4) | 2,27 | 14,25 | 2,79 | 1,011 | 0,9944 | 1,0247 | 0,6845 | 2,91 | 78 |
| CW1(5) | 2,22 | 14,18 | 2,89 | 1,0115 | 1,0035 | 1,0336 | 0,6925 | 2,93 | 78 |
| CW1(6) | 2,28 | 14,26 | 2,79 | 1,0156 | 1,0046 | 1,0349 | 0,6915 | 2,93 | 78 |
| CW2(1) | 2,31 | 14,12 | 2,78 | 1,0089 | 0,9996 | 1,056 | 0,7251 | 3,011 | 77 |
| CW2(2) | 2,2 | 14,18 | 2,93 | 1,0187 | 1,0079 | 1,066 | 0,7302 | 2,99 | 77 |
| CW2(3) | 2,17 | 14,11 | 2,96 | 1,005 | 0,9827 | 1,041 | 0,7113 | 2,97 | 77 |
| CW2(4) | 2,174 | 14,16 | 2,95 | 1,0101 | 1,0021 | 1,0601 | 0,7263 | 2,99 | 77 |
| CW2(5) | 2,23 | 14,18 | 2,87 | 1,0104 | 1,0037 | 1,0614 | 0,7282 | 3 | 77 |
| CW3(1) | 2,23 | 14,35 | 2,98 | 1,0773 | 1,0645 | 1,104 | 0,7159 | 2,74 | 75 |
| CW3(2) | 2,23 | 14,39 | 2,98 | 1,0814 | 1,0777 | 1,1152 | 0,7288 | 2,78 | 75 |
| CW3(3) | 2,28 | 14,34 | 2,98 | 1,0965 | 1,0826 | 1,122 | 0,731 | 2,76 | 75 |
| CW3(4) | 2,29 | 14,37 | 2,93 | 1,0976 | 1,0893 | 1,1029 | 0,7202 | 2,78 | 76 |
| CW3(5) | 2,83 | 14,37 | 1,67 | 0,7684 | 0,6068 | 1,1327 | 0,7362 | 2,74 | 75 |
| CW4(1) | 2,28 | 14,22 | 2,95 | 1,0686 | 1,0541 | 1,0994 | 0,7387 | 2,91 | 76 |
| CW4(2) | 2,22 | 14,22 | 2,96 | 1,045 | 1,0386 | 1,0869 | 0,7289 | 2,89 | 76 |
| CW4(3) | 2,29 | 14,18 | 2,95 | 1,0669 | 1,0513 | 1,105 | 0,7403 | 2,87 | 75 |
| CW4(4) | 2,28 | 14,2 | 2,98 | 1,0802 | 1,0652 | 1,109 | 0,7449 | 2,91 | 76 |

Coated SiC whisker-Alumina Composites

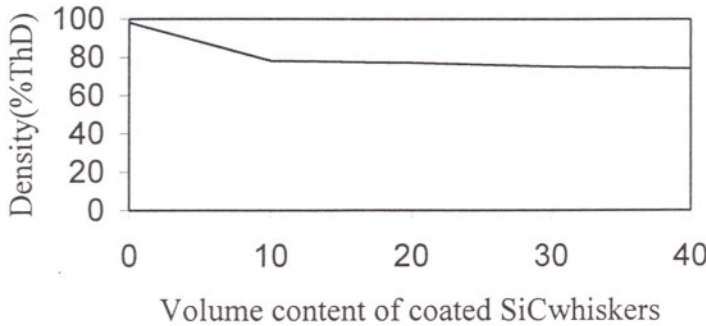


Figure 43. Effect of coated SiC whiskers on densification of Alumina matrix composites.

Table 5. Effect of 1100C calcined coated SiC particulates on sintering for 1 hour

| Sample No | Green Density g/cm ³ | Dg (mm) | hg (mm) | Wg (g) | Wd (g) | Ws (g) | Wss (g) | intered Density g/cm ³ | %thd |
|-----------|---------------------------------|---------|---------|--------|--------|--------|---------|-----------------------------------|------|
| CP1(1) | 2.22 | 14.22 | 2.9 | 1.022 | 1.009 | 1.021 | 0.7343 | 3.508 | 90 |
| CP1(2) | 2.24 | 14.19 | 2.83 | 1.004 | 0.995 | 1.006 | 0.7188 | 3.45 | 88 |
| CP1(3) | 2.23 | 14.16 | 2.78 | 0.977 | 0.964 | 0.977 | 0.6953 | 3.42 | 87 |
| CP2(1) | 2.18 | 14.1 | 2.31 | 0.785 | 0.779 | 1.022 | 0.7301 | 2.67 | 70 |
| CP2(2) | 2.05 | 14.18 | 2.26 | 0.731 | 0.726 | 0.761 | 0.5156 | 2.95 | 77 |
| CP2(3) | 2.19 | 14.15 | 2.61 | 0.898 | 0.893 | 0.937 | 0.6337 | 2.93 | 77 |
| CP3(1) | 2.16 | 14.18 | 2.9 | 0.988 | 0.971 | 1.041 | 0.6878 | 2.74 | 73 |
| CP3(2) | 2.14 | 14.03 | 2.1 | 0.704 | 0.695 | 0.745 | 0.4914 | 2.74 | 73 |
| CP3(3) | 2.12 | 14.08 | 2.94 | 0.998 | 0.99 | 1.059 | 0.7 | 2.75 | 74 |
| CP4(1) | 2.05 | 14.16 | 2.25 | 0.744 | 0.733 | 0.793 | 0.5132 | 2.61 | 71 |
| CP4(2) | 2.04 | 15.1 | 2.7 | 0.994 | 0.988 | 1.079 | 0.6912 | 2.54 | 69 |
| CP4(3) | 2.07 | 14.13 | 2.84 | 0.943 | 0.94 | 1.015 | 0.6551 | 2.59 | 71 |

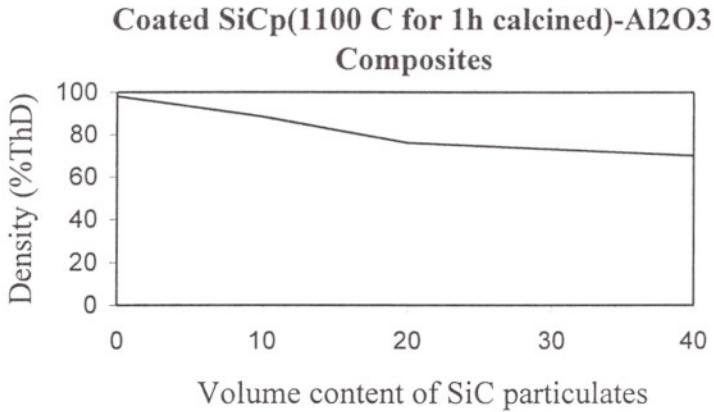


Figure 44. Effect of 1100C calcined coated SiC particulates on densification of Alumina matrix composites.

Table 6. Effect of 1100C calcined coated SiCwhisker on Sintering

| Sample No | Green Density g/cm ³ | Dg (mm) | hg (mm) | Wg (g) | Wd (g) | Ws (g) | Wss (g) | Sintered Density g/cm ³ | %thd |
|-----------|---------------------------------|---------|---------|--------|--------|--------|---------|------------------------------------|------|
| CW1(1) | 2.21 | 14.1 | 2.88 | 0.994 | 0.977 | 1.0305 | 0.7215 | 3.15 | 81 |
| CW1(2) | 2.2 | 14.1 | 2.98 | 1.015 | 1.002 | 1.0537 | 0.7315 | 3.11 | 80 |
| CW2(1) | 2.11 | 14.21 | 2.95 | 0.989 | 0.98 | 1.0675 | 0.7069 | 2.71 | 71 |
| CW2(2) | 2.11 | 14.13 | 3.01 | 0.998 | 0.987 | 1.0822 | 0.7132 | 2.67 | 70 |
| CW3(1) | 2.02 | 14.29 | 3.05 | 1.037 | 1.022 | 1.1402 | 0.7276 | 2.48 | 66 |
| CW3(2) | 2.35 | 14.2 | 2.95 | 0.997 | 0.99 | 1.1014 | 0.7036 | 2.48 | 66 |
| CW3(3) | 2.12 | 14.18 | 2.97 | 1 | 0.993 | 1.1044 | 0.7065 | 2.49 | 66 |
| CW4(1) | 2.07 | 14.26 | 3.28 | 1.051 | 1.028 | 1.145 | 0.7189 | 2.412 | 66 |
| CW4(2) | 2.08 | 14.27 | 3.1 | 1.057 | 1.021 | 1.1438 | 0.7144 | 2.378 | 65 |
| CW4(3) | 2.05 | 14.21 | 3.38 | 1.092 | 1.071 | 1.2046 | 0.7493 | 2.352 | 64 |

1100C calcined coated SiCwhisker-Alumina Composites

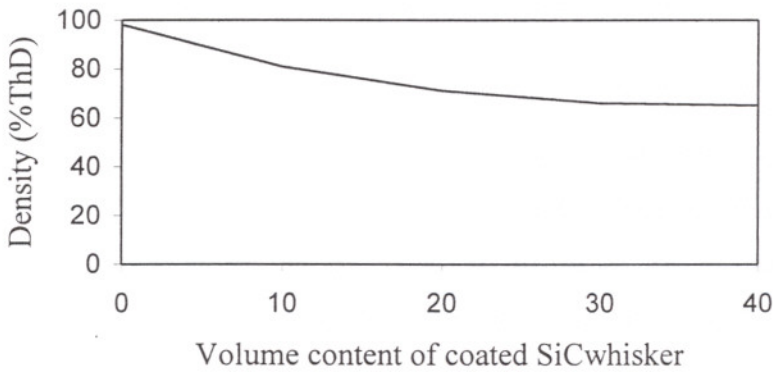


Figure 45. Effect of 1100C 1h calcined coated SiCwhiskers on densification of Alumina matrix composites.

6.4 Thermal Analysis

Thermogravimetric analysis (TGA) up to 1000⁰C was carried out on the uncalcined aluminium sulfate hydrate coated SiCp and SiCw samples shown in Figure 46 and in Figure 47, respectively. Percentage weight loss was also determined for these samples calcined to various temperatures in the range 250⁰ to 1000⁰C in a static air atmosphere at a heating rate of 10⁰C/min, 5⁰C/min and 2⁰C/min. Similar results are obtained in Figure 46 and 47. The differences between three curve shown in Figure 47 were due to the using different amount of powder. The similar curves were obtained in Figure 46 were due to the using same amount of powder. The weight loss for the 1000⁰C calcined SiCp and SiCw was ~34 %wt the 250⁰C coated SiCp and SiCw samples showed half of this loss i.e ~20 %wt and ~19 %wt, respectively. This behaviour indicated that the both precipitated materials are hydrated. They contain molecular water. Aluminium sulfate hydrate deposited on SiCp and SiCw tended to lose hydration water at relatively low temperatures. Kato et al (15) dehydrated several aluminium sulfates at temperatures in the range 200⁰C to 400⁰C

The weight loss for the 450⁰C calcined coated SiCp and SiCw samples were ~25 %wt and ~24 %wt respectively. These percentages only increased to ~28 %wt and ~26 %wt for the 800⁰C calcined coated SiCp and SiCw samples, respectively. Studies on the dehydroxylation of boehmite (AlOOH) in the temperature range ~400⁰ to 600⁰C showed relatively small weight loses (15). Small endothermic peak was observed in the DTA (Figures 50 and 51) in the temperature range ~700⁰C to 800⁰C. This behaviour was attributed to dehydroxylation and to small amount of desulfurization.

The weight loss increases from ~28 %wt and ~26 %wt for the 800⁰C coated SiCp and SiCw samples to ~33 %wt for the 950⁰C coated SiCp and SiCw samples, respectively. This was consistent with FTIR (Figures 48 and 49) results indicating that substantial desulfurization occurs during this range. A large weight loss was indicated in the TGA curve in the temperature range 800⁰C to 950⁰C. Samples calcined at temperatures above 950⁰C showed small

additional weight losses. The FTIR results revealed that these losses were associated with residual sulfate decomposition.

İZMİR YÜKSEK TEKNOLOJİ ENSTİTÜSÜ
REKTÖRLÜĞÜ
Kütüphane ve Dokümantasyon Daire Bşk.

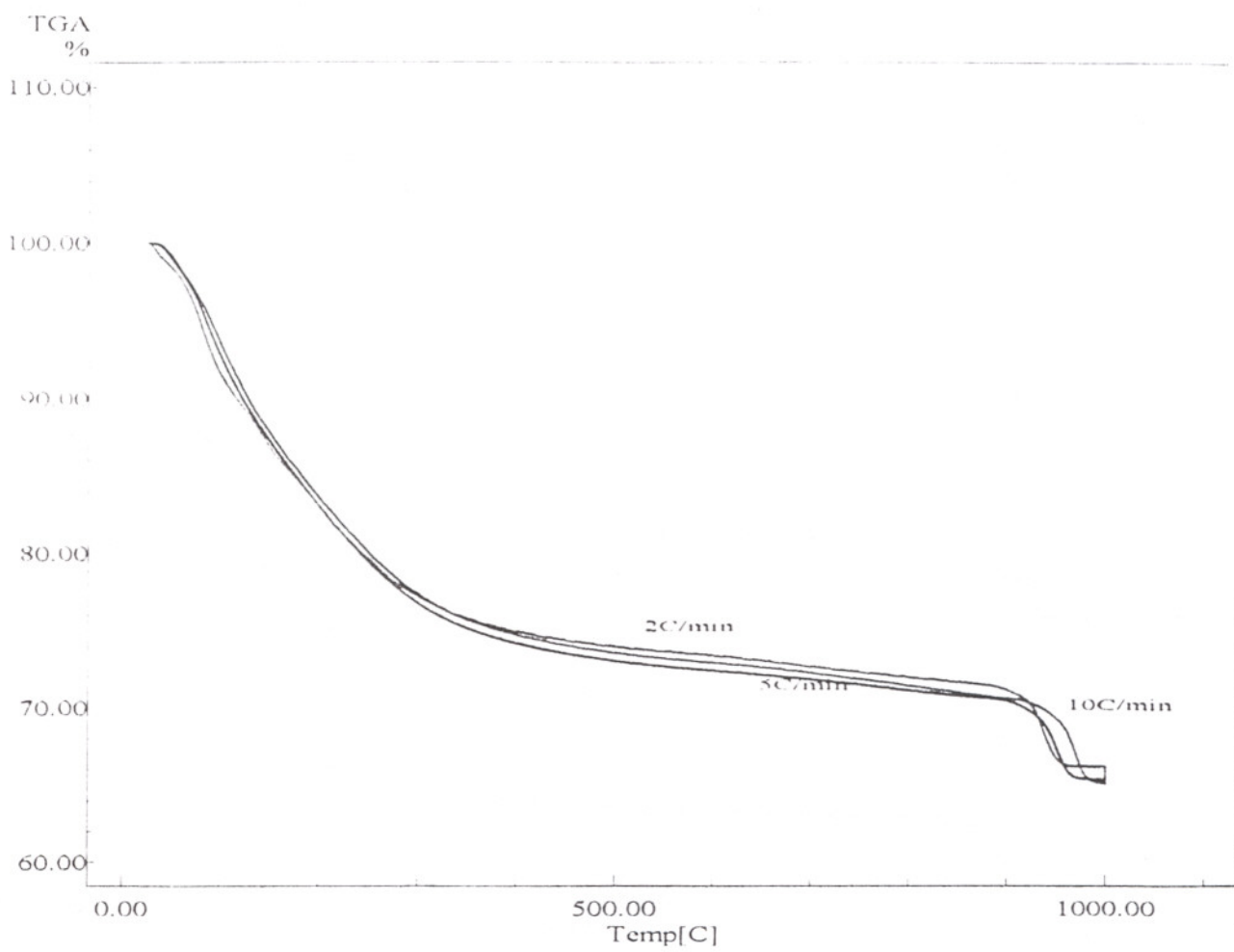


Figure 46. TGA curve for coated SiC particulates

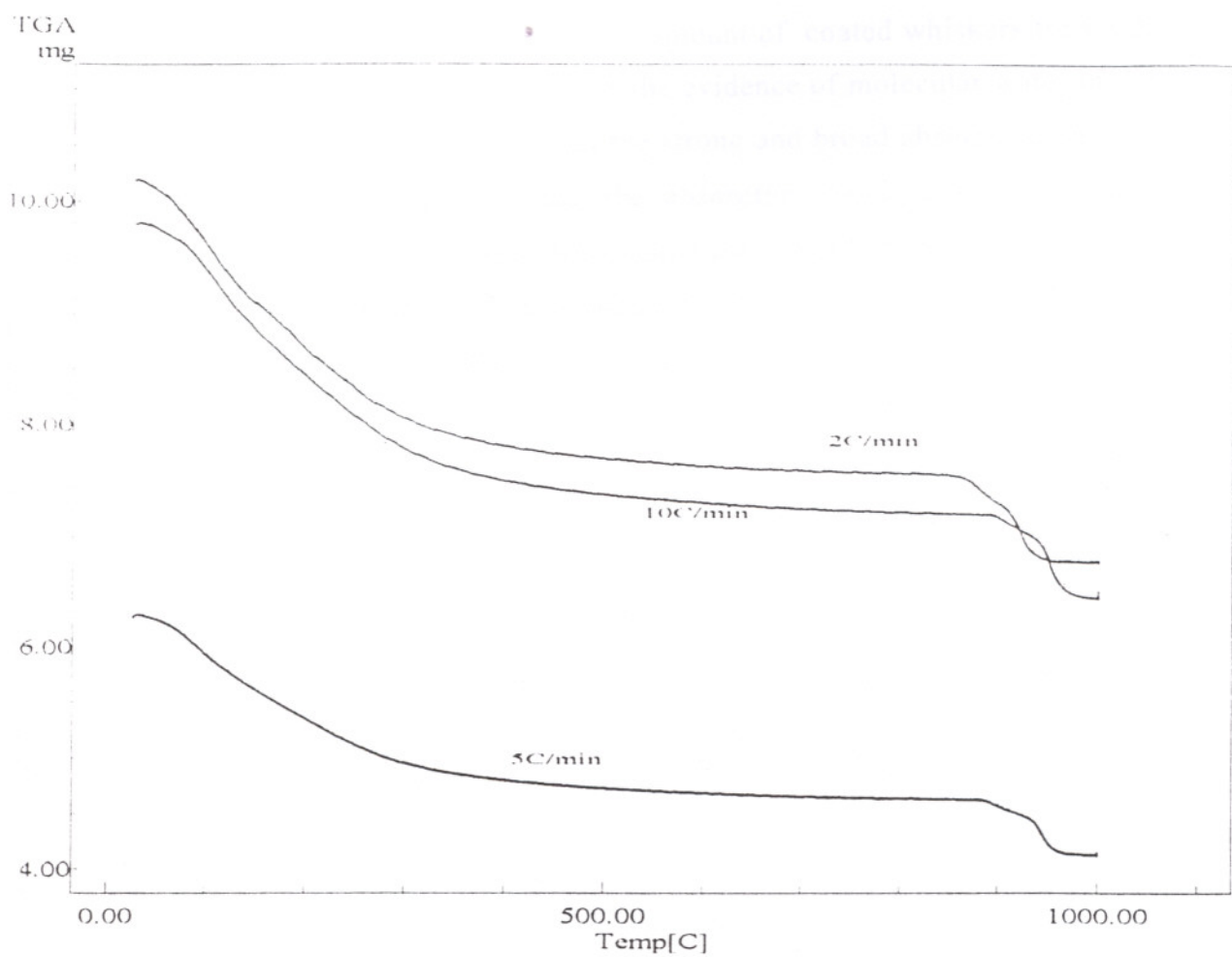


Figure 47. TGA curve for coated SiC whiskers

6.5 Chemical Characterization

The XRD pattern in Figure 34 shows that the coating material on the SiC particulates is amorphous. The FTIR spectrum for SiC particulates and SiC whiskers are shown in Figure 48 and 49, respectively. Both spectra gave similar results. The peak intensities of coated whiskers were low than that of the coated particulates. This difference between two spectra was due to the using different amount of powder. It was used almost half amount of coated whiskers for FTIR spectrum. The small peak at 1610 cm^{-1} is the evidence of molecular water in the structure. Sacks et al (25) reported that the strong and broad absorption band in the region ~ 3150 to 3550 cm^{-1} and the absorption band at 1655 cm^{-1} are observed from the FTIR spectrum for uncalcined sample (Figures 48 and 49). This is the evidence of molecular water in the structure. From the FTIR spectrum in (Figures 48 and 49), small dehydration peak is observed due to the drying of the sample at 70°C . The small peak at 970 cm^{-1} is due to the sulfate absorption. Similar result was obtained by Sacks et al (25). They reported that the strong band centered at 1120 cm^{-1} and small peak at 980 cm^{-1} observed from FTIR spectrums were attributed the sulfate absorption. In contrast, an absorption band at 1230 cm^{-1} in an uncalcined crystalline basic aluminium sulfate is associated with the O-H bending vibration of "free" hydroxyl group. From the Figures 48 and 49 the peak at $\sim 1138\text{ cm}^{-1}$ is associated with dehydroxylation rather than sulfate absorption (discussed below).

At 250°C , the FTIR spectrum was similar to the 70°C spectrum although some dehydration was indicated. The band centred at 1610 cm^{-1} was substantially reduced in comparison to the 70°C -dried sample.

Dehydration was also indicated by DTA results for coated SiC particulates and SiC whiskers in Figures 50 and 51. The small exothermic peak due to the 70°C dried samples were analyzed from the initial heating (above room temperature) to 400°C , with peak at 120°C . This relatively low temperature indicated that the dehydration process was associated with molecular water rather than dehydroxylation.

Although decomposition was dependent upon factors such as calcination time-temperature schedule and atmosphere, crystallite size, specific phases present, etc., the major endothermic DTA peak in aluminium hydroxides were generally observed at higher temperatures, ie in the range 250⁰C to 550⁰C (Figures 50 and 51) (25).

At 400⁰C the FTIR spectrum (Figures 48 and 49) was similar to the 70⁰C and 250⁰C materials. The additional absorption that appeared at ~1138 cm⁻¹ in the 250⁰C material was more pronounced in the 400⁰C material. Similar results were obtained by Sacks et al (25).

Further evidence for the presence of hydroxyl groups in low temperature calcined samples was provided by the small endothermic peak (Figures 50 and 51) in the range ~600⁰C-700⁰C. Since the temperature was too low for the loss of sulfur and too high for the loss of molecular water. This peak was most likely associated with dehydroxylation. Decomposition of various aluminium hydroxides phases usually show endothermic peaks in ~400⁰C- 600⁰C (25).

At 600⁰C and 700⁰C, the peak for the partially dehydrated basic aluminium sulfate on the SiC was observed at 1138 cm⁻¹ for the 600⁰C and 700⁰C sample. This indicated that dehydroxylation completed until temperature range (to be discussed at 6.6).

At 800⁰C and 900⁰C, the sulfate peak at 970 cm⁻¹ for the 800⁰C and 900⁰C samples solved completely. The large endothermic peak also indicated desulfurization at ~1000⁰C, in the DTA (Figures 50 and 51).

Above 900⁰C, the peaks in the range ~400 to 900 cm⁻¹ solved completely, indicating that extensive crystallization has occurred. The FTIR spectra (Figures 48 and 49) showed that additional desulfurization occurs between 1000⁰C and 1100⁰C.

The transformation proceeds with several intermediate phases (γ, η, \dots) in most hydroxide-derived alumina's (25). δ or θ alumina which are common transition phases did not indicate directly during the conversion from γ -Al₂O₃

to α - Al_2O_3 . The FTIR spectrums (Figures 48 and 49) showed also that additional desulphurisation occurs between 1000°C and 1100°C .

The exothermic peak at $\sim 1300^\circ\text{C}$ in the DTA curves (Figures 50 and 51) reflected the γ - α transformation. The FTIR spectrums for 1100°C samples indicated a small residual sulfate content in the coating. This was consistent with previous observations of sulfate in alumina to temperatures above 1100°C (25). Increased peaks in the range ~ 400 to 900 cm^{-1} were correlated with the γ - α transformation in the coating material.

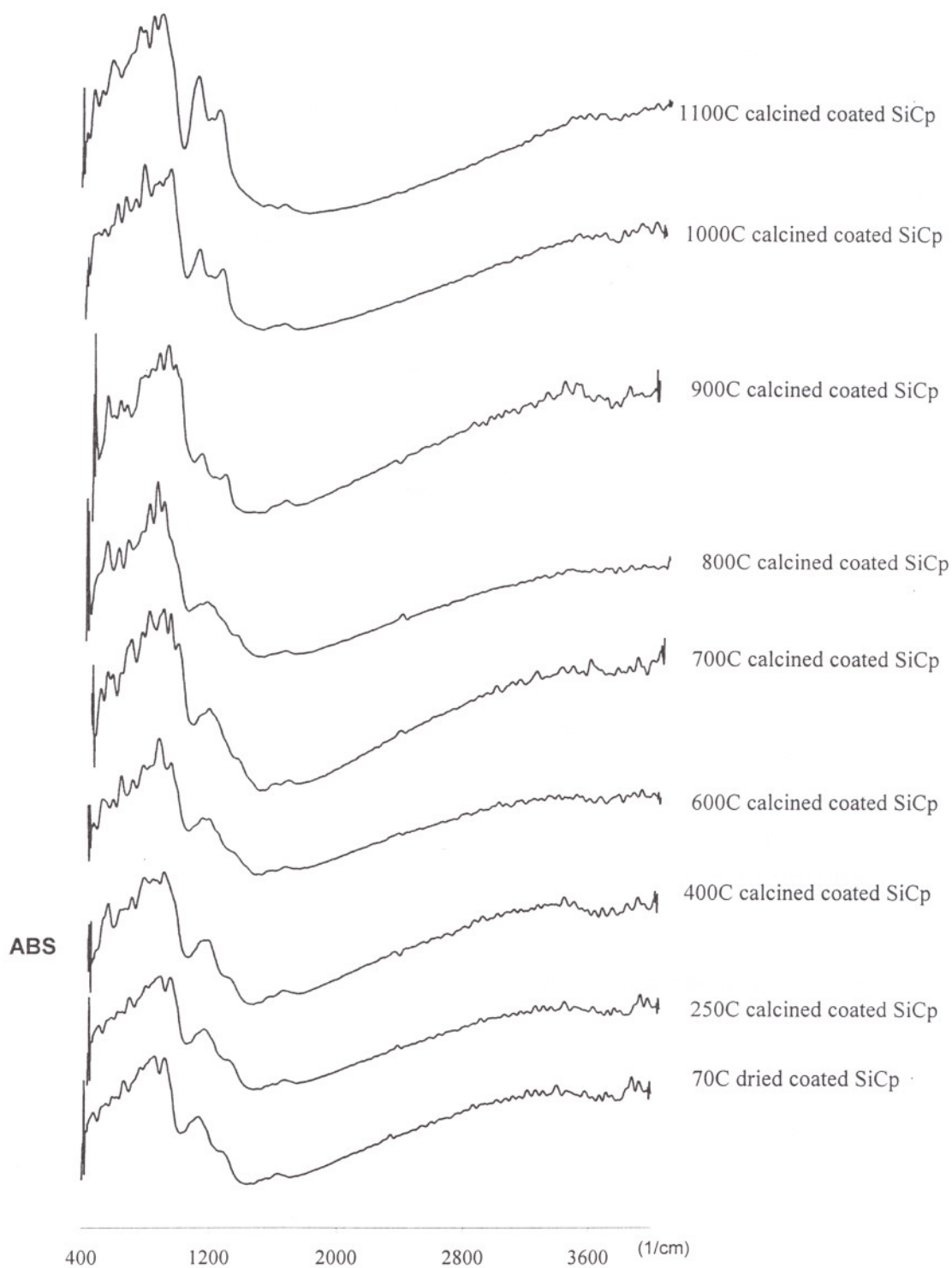


Figure 48. FTIR spectrum of coated SiC particulates.

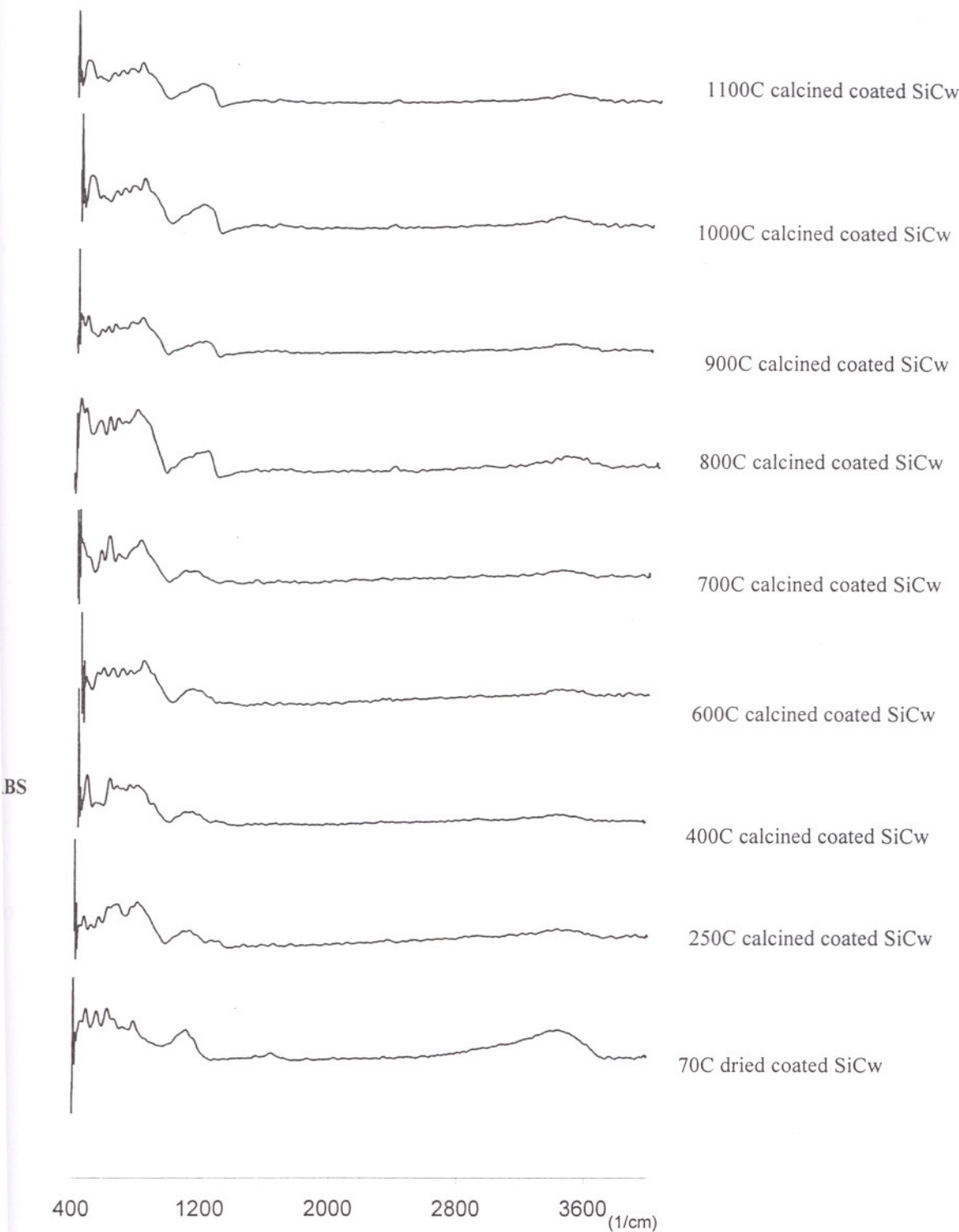


Figure 49. FTIR spectrum of coated SiC whiskers.

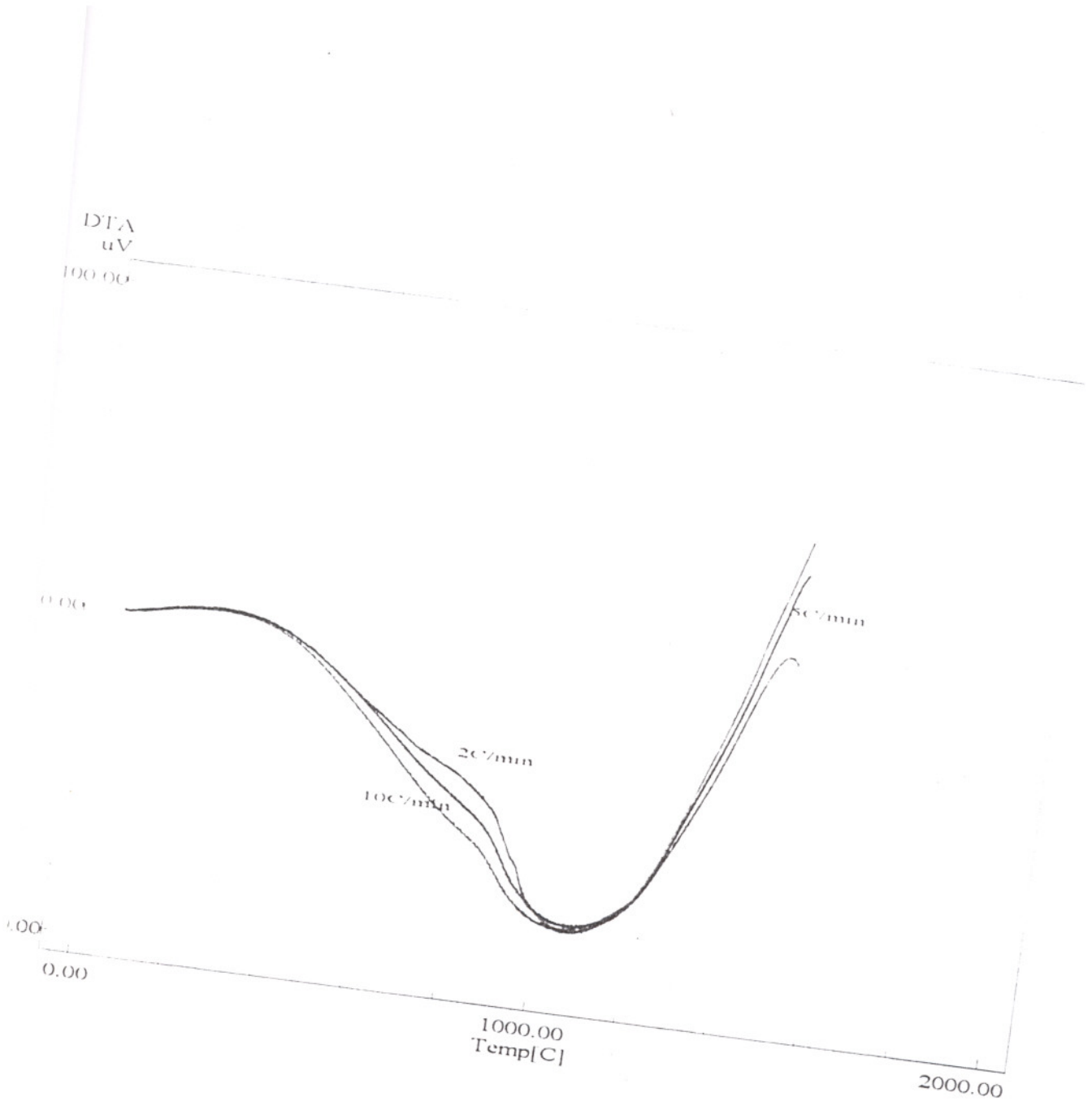


Figure 50. DTA curve for coated SiC particulates

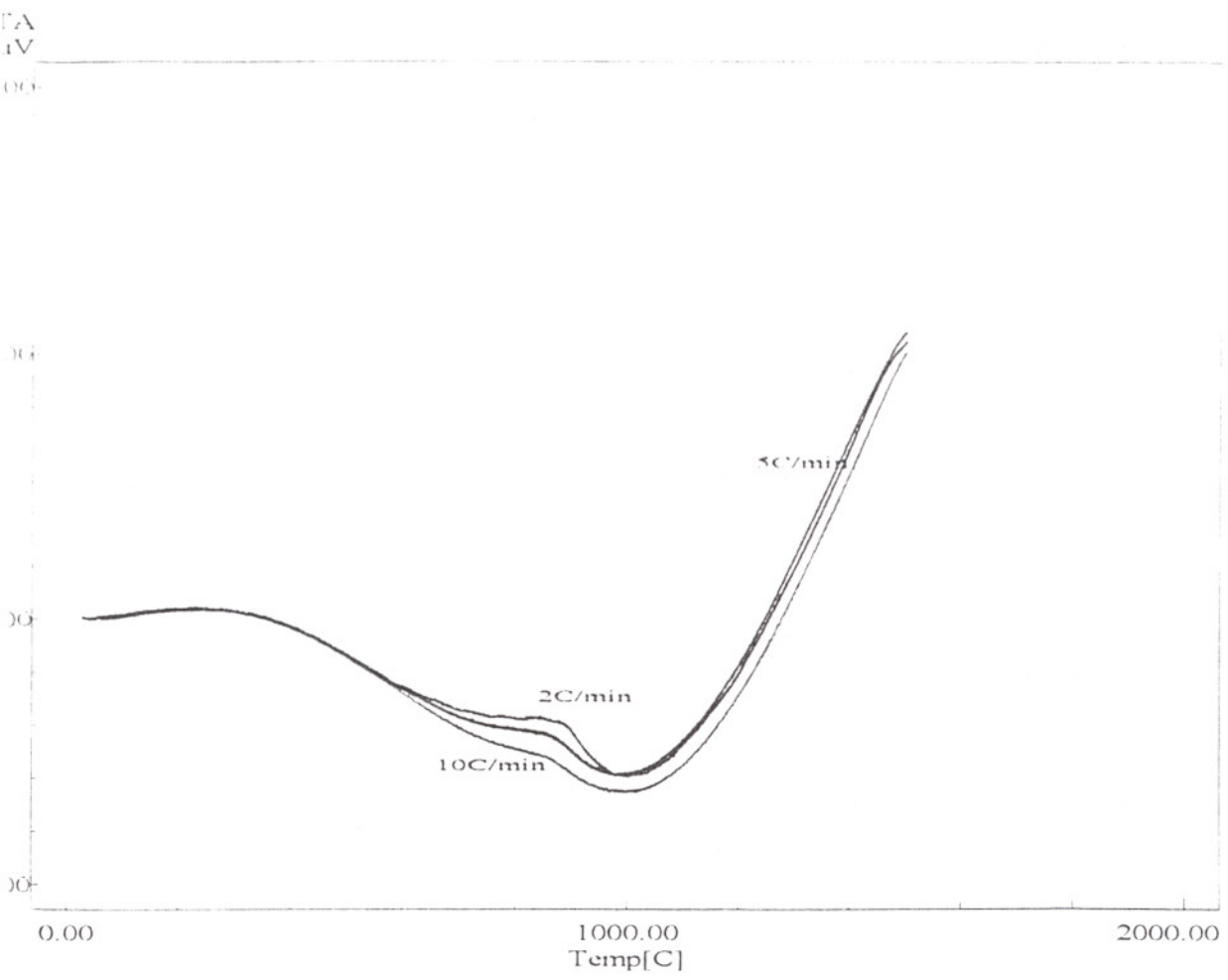


Figure 51. DTA curve for coated SiC whisker

6.6 Vickers Microhardness Test Results

The microhardness values of SiC-Al₂O₃ composites at different SiC volume content are shown in Table 7.

Table 7. Vickers Microhardness Test results of the SiC- Al₂O₃ Composites.

| SAMPLE NO | INDENTOR | INDENTATION | VICKERS HARDNESS |
|--|----------|-------------|------------------|
| | LOAD (N) | TIME (sec) | (GPa) (AVE) |
| %20uncoatedSiCp-Al ₂ O ₃ | 9.8 | 15 | 6.39 |
| %20coated SiCp-Al ₂ O ₃ | 9.8 | 15 | 10.71 |
| %30coated SiCp-Al ₂ O ₃ | 9.8 | 15 | 12.94 |
| %20 coated SiCw-Al ₂ O ₃ | 9.8 | 15 | 10.89 |
| %40 coated SiCw-Al ₂ O ₃ | 9.8 | 15 | 5.96 |

Gritsenko and Kilsly (10) have reported the hardness of oxide ceramics as 14.5-21 GPa. They have given the vickers microhardness value of Al₂O₃ which is 20 GPa. However, Harmer et al (11) reported the microhardness value of alumina as 17.3 GPa. Vickers microhardness of sintered alumina (AKP50 Sumitomo) which has 98.8% theoretical density was measured 14.92 GPa with 9.8N indentation load (Figure 37). Related with SiC-Al₂O₃ composite specimen, the microhardness values obtained from the literature shows similar characters. Nutt et al (20) have measured the hardness values of SiC_w-Al₂O₃ composites with 10 kg indentation load as 20.7 and 23.2 GPa. Kobayashi and Deobald (17) have measured the hardness of 5 vol.% SiC- Al₂O₃ composites as 19.2 GPa. In this study, for the SiC-Al₂O₃ composite which are prepared with %20, %30 and

%40 volume percent of SiC, the microhardness values slightly different compared with the literature. The hardness increased with SiC volume content up to a maximum of about 12.94 GPa for the composite containing 30 vol.% SiC particulates. Compared with the uncoated SiCp- Al₂O₃ composite, the increasing of the hardness was observed from the Table 7. In the whisker composites, the hardness decreased as the whisker content increased to 40 vol.%. The low hardness of the uncoated 20 vol.% SiCp- Al₂O₃ and coated 40 vol.% SiCw- Al₂O₃ composites were attributed to their low densities. This difference related with composite microhardness values may come from the differences in the microstructures of the specimen and percentage composition of the composite structure (percentage of the SiC in alumina matrix). Also there is big difference in the indentation load and the time which is applied during the hardness test between this study and reported previous studies. Although the indentation load does not effect the hardness result in Vickers Hardness method, the difference between the 100-200N and 0.98N indentation load may cause different results. Similarly indentation time is also important. Hardness test use big amount of indentation load at sufficiently long indentation time. But in the microhardness testing indentation time is approximately 15 sec. In recent studies the authors reported the hardness values in wide scale. This scale includes both hardness and microhardness values (17) . For example in the range 2-200N can give more accurate results for hardness value of the specimen.

CONCLUSIONS AND RECOMMENDATIONS

Precipitation of hydrated aluminium sulfate was the successful method for producing an alumina powder precursor under experimental conditions. At higher excess use of urea, many spherical particles were seen. In addition, at high concentrations of aluminium sulfate, the spherical shape and uniformity of size were not preserved. Spherical particles coated the SiC whiskers and particulates with the change of pH through out the solution. The particle size of the precipitate increased with the increasing pH. Although these particles were coagulated heavily around pH=4, the system became dispersed at higher pH values (pH>5.5). The XRD result showed the coating of the samples at pH \cong 6.47 is amorphous. On the other hand, when the reaction was continued up to pH= 8.7; the alumina hydrate on the SiC whiskers and particulate crystallized into pseudo boehmite and separated from SiC whiskers and particulates.

The thermal expansion coefficient of SiC is almost half of the alumina matrix. This difference within the thermal expansion coefficients causes pull stress in the matrix during sintering. SiC whiskers interfere with the shrinkage of the surrounding the matrix. This is the most important reason of low density of SiC-Al₂O₃ composites. In order to prevent thermal stresses caused by thermal expansion coefficient mismatch between the matrix and second phase and microcracks and large pores, the whiskers and particulates were coated with Al-SO₄-OH precursor. Upon heating the precursor transformed to α -Al₂O₃ by providing empty spaces for matrix densification during the sintering process. SEM pictures showed large holes in the both particulate and whisker composite structures. It may occur due to the agglomeration of whiskers and particulates in the matrix. The distribution of the coated SiC in the matrix should be studied for these composites in future.

In this work, the density of both uncoated SiC whiskers and particulates were low compared with the literature. This may be due the distribution of second phase in the matrix. The density of the coated SiC- Al₂O₃ composites containing 10-40 vol% SiC was compared with the uncoated SiC- Al₂O₃

composites at the same volume content. The density of composites prepared with alumina hydrate coated SiC whiskers and particulate were almost 22 % greater than that of the density of composites prepared with uncoated SiC particulate and whiskers. This result may show that the coating have gained time for matrix densification and so provide dense composites (shrink-fit idea) or the improvement of the distribution of second phase in the matrix may be obtained.

The density of these composites slightly decreased as the whisker/particulate content increased from 10 to 40 vol%. For instance, the density of 10 vol% SiCp- Al₂O₃ was 3,16 when the density of 40 vol % SiCp- Al₂O₃ was 2.64. The decreasing density of composites were attributed to the increasing reinforcement phase content and large holes caused by the thermal expansion coefficient mismatching between the matrix and reinforcement phase and agglomerated SiC whiskers/particulates.

In this study thermal properties of coated SiC whiskers and particulate were investigated by using TGA and DTA. Thermogravimetric analysis (TGA) up to 1000⁰C was carried out on the uncalcined aluminium sulfate hydrate coated SiCp and SiCw samples. The weight loss for the 1000⁰C calcined SiCp and SiCw was ~34%wt, the 250⁰C calcined coated SiC samples showed half of this loss ie ~20%wt. This behaviour was indicating that the both coated SiCw and SiCp were hydrate. In the temperature range ~700⁰C to 800⁰C, the small endothermic peak was observed in the DTA curve and the small weight loss was obtained from the TGA curve. This behaviour was attributed to dehydroxylation. From 800⁰C to 950⁰C, the weight loss observed in TGA curve increased and in the DTA curve large endothermic peak appeared. This was consistent with FTIR results indicating that substantial desulphurization occurred during this range.

The mechanical performances of these composites were measured by using Vickers Microhardnes Testing Devices. Vickers microhardness of the 20vol.% and 30vol.% coated SiCp ,and 20vol.% and 40 vol.% SiCw-Al₂O₃ composites were measured as 10.71, 12.94, 10.89 and 5,96 Gpa, respectively. In this study, for the SiC- Al₂O₃ composites which are prepared with %20, %30

and %40 volume percent of SiC, the microhardness values are slightly different, compared with the literature. This was attributed to their low density. This difference related with composite microhardness values may come from the differences in the microstructures of the specimen and indentation load time and volume content of second phase.

İZMİR YÜKSEK TEKNOLOJİ ENSTİTÜSÜ
REKTÖRLÜĞÜ
Kütüphane ve Dokümantasyon Daire Bşk.

APPENDIX

Sample Calculations for the Density Measurement

1. *Density measurement calculation for porous sample:*

$$\rho^* = \left(\frac{W_d * \rho_{fluid}}{(W_s - W_{ss})} \right)$$

2. *Relative density calculation:*

$$\text{ThD}\% = (\rho_s / \rho_{\text{THEO}}) \times 100$$

W_D = Dry Weight of the sample (1) (Figure 52).

G = Weight in water with out any process (2) (Figure 52).

W_S = Saturated weight (1) (The sample was kept for half of an hour in boiling water then it let to cool in water. The liquid film was removed with a wet handkerchief and measurement was done)

W_{SS} = Weight in water after the process (2) (Figure 52).

ρ_f = Density of water

ρ_s = Density of sample

ρ_{THEO} = Theoretical density of the sample

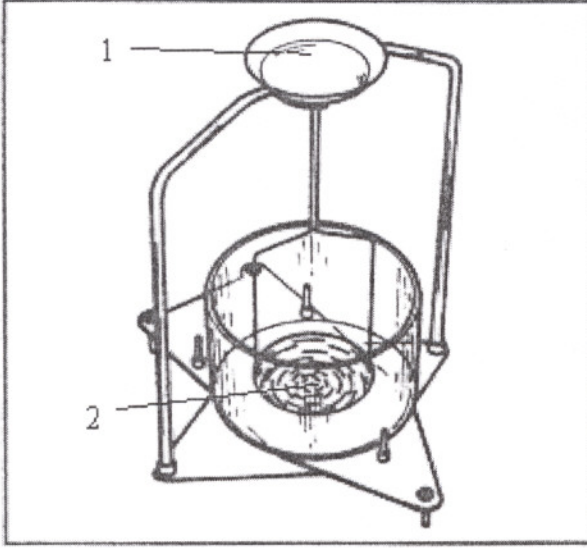


Figure 52. A schematic illustration for the density measurements (Sartorius YD01 density measurement kit).

REFERENCES

1. Baek V. K., Kim C. H., *J. Mater. Sci.* 24 (1989) 1589-1593
2. Barclay S. J., Fox J. R., Bowen H. K., "Processing of Pressureless-Sintered SiC whisker-reinforced Al₂O₃ Composites", *J. Mat. Sci.* 22 (1987) 4403-4406
3. Becher P. F., Wei G. C., *J. Am. Ceram. Soc.* 12, C144-C145
4. Blendell John E., Bowen H. Kent, and Cable Robert L., "High Purity Alumina by Controlled Precipitation from Aluminium Sulphate Solutions", *Ceramic Bulletin*, Vol:63, No:6, 1984
5. Cahn R.W., Haasen P., Kramer E.J., *Materials Science and Technology, Processing of Ceramics*, Vol.17A, 1996, New York
6. Carnie J. A. and et al., "Processing of Metal and Ceramic Matrix Composites", *Ceramic Bulletin*, 65 (1986) 293-304
7. Evans A.G., "The mechanical properties of reinforced ceramic, metal and intermetallic matrix composites", *Mater. Sci. and Eng.*, A143 (1991) 63-76
8. Faber K.T., "CERAMIC COMPOSITE INTERFACE : Properties and Design", *Annu. Rev. Mater. Sci.*, 1997, 27:499-524
9. Giannakopoulos Antonios E., Breder Kristin " Synergism of Toughening Mechanism in Whisker-Reinforced Ceramic-Matrix Composites", *J.Am.Ceram.Soc.*,74(1) 194-202(1991)
10. Gritsenko E.I., Kisly P.S., "Superhard Materials for Cutting Operations", *Ceram.Soc.*, 71(6) 503-512 (1988)
11. Harmer M., Chan M., Khan A., "Toughness-Curve Behavior of an Alumina Mullite Composite", *J.Am.Ceram.Soc.*,81(10) 2613-23(1998)
12. Huang Z., Jiang D., and Tan S., " Colloidal Processing of SiC Whisker Composites", *J.Am. Ceram. Soc.*, 78 (1995) 2240-42
13. Internet Explorer
14. Kapolnek D., Dejonghe L.C.," Particulate Composites from Coated Powders", *J.Eur. Ceram. Soc.*, 7 (1991) 345-51

15. Kato S., Daimon A., and Nanbu M., "Decomposition of two Aluminium Sulfates and Characterization of Resultant Aluminas", *J.Am.Ceram.Soc.*, 64(8) 436-43
16. Kingery W. D., Bowen H. K., Uhlmann D. R., *Introduction to Ceramics*, 1976, Canada
17. Kobayashi S.A., and Deobald L., "Impact Testing of Al₂O₃ and Al₂O₃-SiC Composite", *Fracture Mechanics: Volume 24*
18. Nakamura H., Kato A., "Effect of Crystallization of Alumina Hydrate in Preparation of Alumina-coated Composite Particles" *Ceram. Inter.*, 18(1992)201-206
19. Naslain Roger R., "The design of the fibre-matrix interfacial zone in ceramic matrix composites", *Composites Part A29A* (1998) 1145-1155
20. Nutt R.S., Suresh S., Morrone A.A., "Fracture Toughness and Fatigue Crack Growth Behavior of an Al₂O₃-SiC Composite, *J.Mat.Sci.* 23(1998) 3206-3213.
21. Petrovic J. J., Milewski J. V., Rohr D. L., Gac F. D., *J. Mater. Sci.* Vol:20, 1167-1177 (1985)
22. Reed James S., *Principles of Ceramic Processing, Second Edition*, 1995, New York
23. Rice R.W., "Processing of Advanced Ceramic Composites", *Mat. Res. Soc. Symp. Proc.* Vol:32, 1984
24. Richerson David W., *Modern Ceramic Engineering Properties, Processing, and use in Design*, Second Edition, 1992, New York
25. Sacks Michael D., Tseung-Yuen Tseng and Soo Young Lee, "Thermal Decomposition of Spherical Hydrated Basic Aluminium Sulfate", *Ceramic Bulletin*, Vol:63, No:2, 1984
26. Schwartz Mel, *Handbook Structural Ceramics*, 1992, USA
27. Smith Stanley M., Singh Jitendra P., "Processing and Characterization of SiC-Whisker-Reinforced Alumina Matrix Composites" *J.Am.Ceram.Soc.* 74(2)497-502(1993)
28. Smith William F., *Foundations of Materials Science and Engineering*, 1993, Singapore

29. Tiags T.N., "Properties of SiC whisker-reinforced Oxide Matrix Composites" *Whisker and Fiber Toughened Ceramics Conference Proceedings*, pp 105-107, Am. Metals Society, Columbus, Ohio 1988
30. Tiags T.N., and Becher Paul F., " Sintered Al₂O₃-SiC-Whisker Composites", *Am. Ceram. Soc. Bull.*, 65 (1987) 339-42
31. Tiags T.N., Becher P.F., and Williams R.K., "Pressureless Sintering of SiC whisker-Reinforced Composites", *ORNL/TM-9673* (1985)
32. Toshio I., " Al₂O₃/SiC Whisker Composites ", *MIT Report*, 1990

İZMİR YÜKSEK TEKNOLOJİ ENSTİTÜSÜ
REKTÖRLÜĞÜ
Kütüphane ve Dokümantasyon Daire Bşk.